Nucl. Fusion **53** (2013) 104019 (21pp) doi:10.1088/0029-5515/53/10/104019

An overview of intrinsic torque and momentum transport bifurcations in toroidal plasmas

P.H. Diamond[1,2], Y. Kosuga[1,12], Ö.D. Gürcan[3], C.J. McDevitt[4], T.S. Hahm[5], N. Fedorczak[6], J.E. Rice[7], W.X. Wang[8], S. Ku[8], J.M. Kwon[1], G. Dif-Pradalier[6], J. Abiteboul[6], L. Wang[1,11], W.H. Ko[1,9], Y.J. Shi[1,9], K. Ida[10], W. Solomon[8], H. Jhang[1], S.S. Kim[1], S. Yi[1], S.H. Ko[1], Y. Sarazin[6], R. Singh[1] and C.S. Chang[8]

[1] WCI Center for Fusion Theory, National Fusion Research Institute, Daejeon 305-333, Republic of Korea
[2] Center for Momentum Transport and Flow Organization and Center for Astrophysics and Space Science, University of California, San Diego, CA 92093-0424, USA
[3] CNRS, Laboratoire de Physique des Plasmas, Ecole Polytechnique, Palaiseau, 91128, France
[4] Los Alamos National Laboratory, Los Alamos, NM 87545, USA
[5] Seoul National University, Seoul 151-744, Republic of Korea
[6] CEA-Cadarache, Saint-Paul-lex-Durance, 13197, France
[7] Plasma Science and Fusion Center, Massachusetts Institute of Technology, Cambridge MA 02139, USA
[8] Princeton Plasma Physics Laboratory, Princeton, NJ 08540, USA
[9] KSTAR, National Fusion Research Institute, Daejeon 305-333, Republic of Korea
[10] National Institute of Fusion Science, Toki-Shi, Gifu, 509-5292, Japan
[11] Huazhong University of Science and Technology, Wuhan, 430074, People's Republic of China
[12] Institute for Advanced Study, Kyushu University, Higashi-Ku, Fukuoka 812-8581, Japan

Received 8 November 2012, accepted for publication 30 January 2013
Published 26 September 2013
Online at stacks.iop.org/NF/53/104019

Abstract
An overview of the physics of intrinsic torque is presented, with special emphasis on the phenomenology of intrinsic toroidal rotation in tokamaks, its theoretical understanding, and the variety of momentum transport bifurcation dynamics. Ohmic reversals and electron cyclotron heating-driven counter torque are discussed in some detail. Symmetry breaking by lower single null versus upper single null asymmetry is related to the origin of intrinsic torque at the separatrix.

(Some figures may appear in colour only in the online journal)

1. Introduction

This overview (OV) surveys recent developments in the theory and phenomenology of intrinsic torque. By intrinsic torque we refer both to fluctuation-driven *torque density*, which drives a *local* toroidal flow, and to the *net* fluctuation-driven torque, which drives *global toroidal rotation*. Not surprisingly, boundary torques and other effects play a special role in the dynamics of net toroidal spin-up. Concern with intrinsic torque has been driven by the surge of interest in intrinsic rotation—a rare piece of good news for ITER—which is beneficial to macrostability (i.e. rotation near $q = 2$ can mitigate or stabilize RWMs) and to confinement (i.e. toroidal shear flows contribute to $\boldsymbol{E} \times \boldsymbol{B}$ shear suppression of turbulence and are of particular importance to ion transport barriers (ITBs) and to states of reduced profile stiffness). The concept of intrinsic torque emerged from the struggle to understand asymmetries in co-counter torque scans [1] and to explain and predict intrinsic rotation in H-mode plasmas, which is triggered at the L–H transition [2, 3]. This phenomenon, which was first described by the now famous 'Rice scaling' [2, 4] $\Delta V \sim \Delta W/I_p$, appears to be due to the build-up of a co-intrinsic torque in the H-mode pedestal. Interestingly, a similar rotation increment is observed in I-mode plasmas [5, 6]. Here

I-mode is the improved confinement regime which sometimes is encountered below the L → H transition threshold. Pedestal structure, specifically the strong radial inhomogeneity due to steep gradients and the boundary, effectively converts the heat flux-driven relaxation ($\sim -Q\nabla T$, the entropy production) to a fluctuation Reynolds stress, which drives the pedestal intrinsic torque density. This theme of heat engine ↔ radial inhomogeneity + symmetry breaking → Reynolds stress → intrinsic torque density is central to intrinsic rotation and will recur many times in this OV. Note that the essence of this approach is to model the intrinsic torque as a heat engine [7, 8], which converts the thermodynamic force $\nabla_r T$, sustained by the heat flux Q, to $\langle V_\phi(r)\rangle$ via some symmetry breaking.

It is important to state that the phenomenology of intrinsic torque is far broader than the familiar Rice scaling paradigm. Indeed, intrinsic (azimuthal) torques have been observed and investigated in basic plasma experiments [9]. More importantly, it is also clearly dynamic and has led to the discovery of new types of transport bifurcation phenomena. These types of bifurcations, which include ohmic reversals and electron cyclotron heating-driven counter torques, have the distinguishing feature that a change in global rotation profile structure occurs without any significant change in confinement. These should be contrasted to the more familiar H-mode or ITB-driven intrinsic rotation [10], where both rotation profiles and confinement (i.e. density and/or temperature profiles) undergo a significant change. Several types of intrinsic torque bifurcation are thought to be related to a possible change in the underlying microturbulence population, which results in a change in direction of the mode group velocity and thus in the non-diffusive stress. These will be discussed in depth here.

We emphasize at the outset that the scope of this OV is limited to intrinsic torque, and that it is *not* a global review of the transport of toroidal momentum. This paper is meant to complement to previous OVs [11, 12], which focused more on 'momentum pinch' modelling. Also, since this paper is an OV, many technical details are omitted. The reader is referred to the original literature for such matters of detail.

The remainder of this paper is organized as follows. Section 2 briefly summarizes the driving phenomenology and basic ideas. Section 3 presents a general formulation of the theory of intrinsic torque and residual stress, in terms of fluctuation entropy dynamics. The heat engine analogy is developed. Section 4 surveys the theory of intrinsic torque from several perspectives. These are: (a) a physical discussion of the most important stress contributions and symmetry-breaking mechanisms, (b) a brief introduction to the gyrokinetic theory of intrinsic torque, (c) a general formulation of the theory of intrinsic torque, as derived from wave kinetics, which provides a useful unified structure, highlights the role of waves in momentum transport, and conveniently highlights the two classes of momentum transport bifurcations, (d) the role of explicit, boundary-related asymmetries on intrinsic torque. In particular, we address the effect of upper single null (USL) versus lower single null (LSN) asymmetry on intrinsic torque, (e) *nonlocal* effects and their possible role in residual stress. We present a general argument as to why intrinsic torque and momentum transport appear 'more nonlocal' than heat transport. Section 5 discusses how the theory fares upon confrontation with the phenomenology. Section 6 contains a critical assessment and discussion of open questions. This includes a section on suggestions for programmatic goals.

2. Basic ideas and driving phenomenology

Historically, early theory and experiments suggested $\chi_\phi \sim \chi_i$ [13, 14]. However, the discovery of intrinsic rotation and the results of perturbation experiments [15, 16] strongly suggested that off-diagonal, non-diffusive components [17, 18] must enter the momentum flux. Thus, we arrive at the basic form of the $\Pi_{r\phi}$ stress tensor, which is [17]

$$\Pi_{r\phi} = \langle n\rangle\langle \tilde{v_r}\tilde{v_\phi}\rangle + \langle \tilde{v_r}\tilde{n}\rangle\langle v_\phi\rangle + \langle \tilde{n}\tilde{v_r}\tilde{v_\phi}\rangle. \tag{1}$$

We do not discuss convection (the 2nd term of the flux) here. Rather little is understood about the $\langle \tilde{n}\tilde{v_r}\tilde{v_\phi}\rangle$ triplet so we do not discuss it here, though there are indications that it may contribute to intrinsic torque in strong turbulence regimes, such as at blob ejection at the edge [19]. The Reynolds stress (i.e. 2nd order, nonconvective part) is given by

$$\langle \tilde{v_r}\tilde{v_\phi}\rangle = -\chi_\phi \frac{\partial\langle v_\phi\rangle}{\partial r} + V\langle v_\phi\rangle + \Pi^R_{r\phi}. \tag{2}$$

Here V is the momentum convection velocity or 'momentum pinch'. The pinch velocity here arises from toroidal effects, which break Galilean invariance. Thus, concerns of Galilean invariance are not relevant. The physics of the pinch velocity $V(r)$ has been exhaustively reviewed elsewhere [11, 12] and will not be discussed here. A useful original reference is by Yoon and Hahm [20]. This leaves $\Pi^{\rm R}_{r\phi}$—*the residual stress*—which is the major focus of this OV. The intrinsic torque density is then $\tau = -\partial_r \Pi^{\rm R}_{r\phi}$. Most generally, $\Pi^{\rm R}_{r\phi}$ is the piece of the Reynolds stress not directly proportional to $\langle v_\phi\rangle$ or $\partial\langle v_\phi\rangle/\partial r$. $\Pi^{\rm R}_{r\phi}$ is then proportional to $\nabla P_{\rm i,e}$, $\nabla T_{\rm i,e}$, or ∇n, and represents the process whereby electron or ion free energy (i.e. stored in radial pressure gradients—the thermodynamic forces) is converted to $\langle v_\phi\rangle$ by the turbulence. $\Pi^R_{r\phi}$ is necessary to spin-up the plasma from rest to a state of stationary rotation, i.e. $\partial_t \int_0^a \langle p_\phi\rangle\,{\rm d}r = nm\chi_\phi\partial\langle v_\phi\rangle/\partial r|_a - nm\Pi^{\rm R}_{r\phi}(a) - nmV(a)\langle v_\phi(a)\rangle$. Here the first term is from the diffusive flux, the second is from the residual stress and the third is from the pinch. Note the diffusive term is negative for co-rotation ($\partial\langle v_\phi\rangle/\partial r < 0$ for $\langle p_\phi\rangle > 0$) and positive for counter-rotation ($\partial\langle v_\phi\rangle/\partial r > 0$ for $\langle p_\phi\rangle < 0$), and acts to oppose the net rotation. Observe that a finite residual stress on the boundary (i.e. $\Pi^{\rm R}_{r\phi}(a) \neq 0$) is required for a net acceleration of the plasma from rest (i.e. from a state with $\langle v_\phi\rangle = \partial\langle v_\phi\rangle/\partial r = 0$). Alternatively, boundary convection of (either sign!) with $\langle v_\phi(a)\rangle \neq 0$ will drive spin-up. The net sign of $V\langle v_\phi(a)\rangle$ determines whether the pinch contribution will be co or counter. The crucial importance of the boundary in intrinsic rotation dynamics is thus apparent. For a no-slip boundary, taking external torque $\tau_{\rm ext} = 0$ and considering a state of zero momentum flux, we obtain the intrinsic velocity profile $\langle v_\phi(r)\rangle = -\int_0^a {\rm d}r'\Pi^{\rm R}_{r\phi}(r')/\chi_\phi(r')$, which directly links intrinsic (i.e. torque free) rotation to $\Pi^{\rm R}_{r\phi}$. Of course, the $\langle V_\phi\rangle$ *profile* is determined by intrinsic torque density $\tau(r) = -\partial_r\Pi^{\rm R}_{r\phi}(r)$, as well as pinch, viscosity, and any external torque present.

Table 1. Selected phenomenology of intrinsic torque

Phenomenon	Signature	Sym. breaking	Key physics	Issue
H-mode and I-mode ETB	spin-up at L → I or H, Rice scaling $v_\phi(0) \sim \nabla T_i, \nabla p_i$	Pedestal $\langle v_E\rangle', I'$	Π_{res} and $\nabla v_\phi \uparrow$ as $\nabla p_i, \langle v_E\rangle \uparrow$ and ETB forms. Cancellation experiment.	Quantitative? ∇T_i or ∇p_i? How achieve global cancellation?
ITB	∇v_ϕ steepens with ∇T_i in ITB with $\tau_{ext} = 0$	$\langle v_E\rangle', I'$ in ITB	π_{res} and $\nabla v_\phi \uparrow$ as $\nabla p_i, \langle v_E\rangle' \uparrow$ Relative hysteresis of $\nabla T_i, \nabla v_\phi$ observed	Quantitative? Relative hysteresis? Role in de-stiffening?
OH inversions	Inversion of $v_\phi(r)$ around pivot for $\nu_* > \nu_{*sat}$. Hysteresis in n, I, B-ramp	Open question $I', \langle v_E\rangle', ...$?	$v_\phi(r)$ invert at $\nu_* \sim \nu_{*OH}$ without observable change in n, T profiles. v_{gr} flip at TEM ↔ ITG transition. → π_{res} flips	Symmetry breaker? Extended flip versus localized flip +spreading Interplay with bndry
Co-NBI H-mode +ECH	ECH + co-NBI → central flattening of v_ϕ	Open question $I', \langle v_E\rangle', ...$?	ECH induces $\Delta\nabla v_\phi(0) < 0$ in NBI H-mode → co NBI + co intr. ped. + cntr ECH. v_{gr} flips at TEM ↔ ITG transition	Density profile peaking? Effect? Extended flip versus localized flip +spreading
LSN ↔ USN L-mode Inversions ∇B asymmetry in P_T	LSN ↔ USN jog → SOL flow reversal → core flow reversal in L-mode ∇B asym. in P_T	SOL flow direction or eddy tilt due combination magnetic and electric field shear	Change in competition between B and E field shear in USL versus LSN. Core responds to bndry +SOL flows	Boundary flow penetration → 'Tail + dog' problem Role of SOL flows?

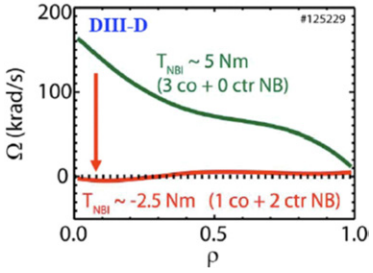

Figure 1. 'Cancellation' experiment of Solomon *et al* from DIII-D [21]. A mix of 1 co and 2 counter beams yield a flat rotation profile with $\langle v_\phi\rangle \cong 0$. This shows that the intrinsic torque for these parameters is approximately that of 1 neutral beam, in the co-current direction.

Regarding the phenomenology of intrinsic torque, an interesting selected subset we discuss here is: (a) H-mode edge transport barrier, (b) ITB, (c) OH-reversal, (d) co neutral beam injection (NBI) H-mode + ECH, (e) LSN↔USN L-mode rotation. This discussion and that of section 5 are summarized in table 1. Of course, the classic example of intrinsic torque and intrinsic rotation is the H-mode electron transport barrier (ETB) [3]. In the absence of external torque, a spin-up is initiated at the L→H transition and builds inwards [3]. The basic trend is described by the Rice scaling $\Delta V_\phi(0) \sim \Delta W/I_p$ where W is energy content and Δ refers to the change across the L→I or L→H transition. The existence and location of the intrinsic torque have been rather convincingly established by the 'cancellation' experiment by Solomon *et al* [21]. The idea here was to exploit the asymmetry between co and counter-NBI H-modes due to the presence of a (hypothetical) 'intrinsic torque' τ. The result, shown in figure 1, is striking: a net counter-torque H-mode yields a rotation profile, which is *flat* (and zero) within the error bars! The implication is clear: the on-axis counter-NBI torque is exactly cancelled by a co-intrinsic pedestal torque! This result *strongly* argues for the viability of the intrinsic torque concept. It also suggests that intrinsic torque can give the appearance of a non-local intrinsic torque phenomenon, in that the intrinsic torque, situated in the pedestal, acts to flatten $\nabla\langle V_\phi\rangle$ in the core. To characterize the pedestal intrinsic torque, data base studies from Alcator C-Mod [8] indicate that central rotation in H-mode and I-mode tracks pedestal ∇T_i, i.e. $V_\phi(0) \sim \nabla T_{i,ped}$, suggesting that the pedestal intrinsic torque is ∇T_i-driven.

Intrinsic rotation in ITBs [22–25] has received *far* less attention than intrinsic rotation in ETBs. This is due in part to the fact that ITBs are usually formed in plasmas subject to external torque. However, since the interaction of external and intrinsic torques is important in low torque scenarios planned for ITER, intrinsic rotation in ITBs and 'de-stiffened' states should receive more attention. Here, a de-stiffened state is one with a stronger response of the temperature gradient to heat flux increments than that exhibited by a stiff state. De-stiffening can be achieved by enhanced $E \times B$ shear, for example. One recent experiment [10] obtained the scaling relation $\nabla V_\phi \sim \nabla T_i$ for intrinsic rotation gradients in ITBs. This is reminiscent of the similar result for ETBs and again suggests that the intrinsic rotation is temperature gradient driven, as in a heat engine. To look beyond correlation to causality, that study investigated *relative hysteresis* between ∇V_ϕ and ∇T_i. Results indicated that hysteresis in ∇V_ϕ was stronger than in ∇T_i, possibly due to the low residual Prandtl number (i.e. $Pr_{resid} \sim \chi_\phi/\chi_i$, in the ITB. Here, χ_ϕ and χ_i are the true, not effective, diffusivities) in the ITB. Since hysteresis of a transport barrier is a consequence of the disparity between transport in the normal and the barrier state, the fact that $\chi_i \gg \chi_\phi$ in the ITB implies that hysteresis will be stronger in ∇v_ϕ than in ∇T_i. Recall $\chi_i \sim \chi_\phi$ in L-mode.

A particularly compelling case for the need to consider intrinsic torque physics is the fascinating phenomenon of rotation reversals in OH or L-mode plasmas. Reversals refer to events in which the global rotation profile spontaneously reverses direction. First studied in detail in TCV [26]

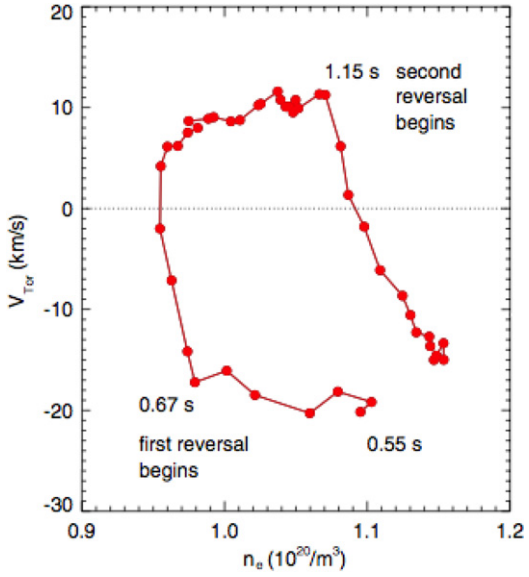

Figure 2. Density ramp hysteresis loop for reversals on Alcator C-Mod [28].

and C-Mod [27–29], reversals are spontaneous 'flips' in the toroidal rotation profile from co to counter (in C-Mod) which occur as n increases and exceeds $n_{\rm sat}$, the density at which confinement transitions from the linear ohmic confinement (LOC) to saturated ohmic confinement (SOC) regime. During the reversal, the rotation profile effectively pivots around a fixed point inside $q \lesssim 3/2$. Interestingly, up–down density ramps reveal back flips, but with some hysteresis, i.e. the velocity versus density plot is a closed loop enclosing finite area, not a straight line, as shown in figure 2. In some cases, a rotation 'spike' (i.e. a transient, spatially localized bump in the toroidal rotation velocity profile) was observed near the edge just after the reversal [28]. Also, experiments on TCV do indicate some differences between reversals in limited and diverted discharges [30], suggesting that the effective boundary conditions play a role in reversal dynamics. Spikes are particularly interesting, as they may hold a clue to the *global* momentum balance and rotation profile dynamics. This is because spikes may reveal the dynamics of momentum ejection events which help understand how the total momentum balance of the core plasma is maintained. Building on the long standing idea that the evolution from LOC to SOC regimes is due to a transition from trapped electron mode (TEM) transport to ion temperature gradient (ITG) transport excited by collisional coupling, a speculation has arisen that inversions are a consequence of a change in the sign of $\Pi^{\rm R}_{r\phi}$ as $n > n_{\rm sat}$ or more generally $\nu_* > \nu_{*\rm crit}$ [31, 32]. This change reflects the dependence of $\Pi^{\rm R}_{r\phi}$ on $v_{\rm gr}$, the group velocity of the underlying microinstability. Alcator C-Mod has pursued fluctuation studies, the results of which are consistent with the expected change in mode populations, but are not conclusive. Further work is needed.

A somewhat related phenomenon, related to the effect of ECH on co-NBI H-mode profiles, has been observed in JT-60U [33], AUG [34], DIII-D [35], KSTAR [36] and HL-2A [37]. Results indicate that ECH of NBI-driven H-modes tends to flatten the otherwise peaked velocity profile, and reduce central rotation speeds ($\Delta V/V \sim -40\%$, in KSTAR), while $\nabla T_{\rm e}$ steepens. Profile studies indicate $\nabla V_\phi \sim \nabla T_{\rm e}$ here, suggestive of a TEM counter-torque in the core. Correlation of ∇v_ϕ and ∇n is also indicated [38]. The H-mode pedestal rotation profile is unchanged by ECH, suggesting that the torque balance here is: co-NBI + pedestal co-intrinsic versus core counter torque related to ECH. KSTAR profiles with NBI and NBI + ECH are shown in figure 3. The data suggest a similar paradigm to that for the OH inversion, namely a change in the direction of the core intrinsic torque from co to counter, due to a flip in mode propagation direction from $v_{*\rm i}$ to $v_{*\rm e}$, as ITG gives way to TEM. Comparative gyrokinetic stability analysis of NBI+ECH and NBI H-modes is, however, somewhat incomplete. This follows from the sensitivity of the results to density profile structure near the pivot radius, and from uncertainty concerning the spatial extent of the region where the mode population flips (according to purely linear analysis). Fluctuation measurements are not yet available. See [34, 36] for more details.

The importance of the edge in intrinsic rotation physics should already be apparent. A classic example of this is the LSN→USN jog experiments of LaBombard in C-Mod L-mode plasmas [39]. Here, 'jog' refers to the process of swing the null point from lower (LSN) to upper (USN) positions by controlled variation of the magnetic configuration. These are often described as a 'tail-wags-the-dog' phenomena, since changes from LSN to USN reverses not only scrape-off layer (SOL) flows, but also the direction of the core rotation. Interestingly, the effect on core rotation vanishes in H-mode, suggesting that the tail is 'cut-off' by the sheared flow in the ETB. The dynamics of this fascinating phenomenon are not understood. In particular, the issue of just how flow changes penetrate from the SOL and boundary to the core remains open. Note that this issue may be related to the long standing mystery concerning the ∇B-drift asymmetry in the L→H power threshold [40]. It is important to note here that at least two types of boundary effects are possible. One is due to SOL flows, produced by up–down SOL asymmetry (i.e. LSN versus USN) and driven by in-out asymmetry of edge particle transport [39]. The other is due to edge stresses, induced by eddy tilting [41].

3. Towards a fundamental theory: intrinsic rotation as the consequence of a heat engine

Recent work [7, 8] has developed a quite general theory of intrinsic rotation as the output of a heat engine, which exploits a heat flux-driven temperature differential (i.e. locally, a temperature gradient ∇T) to drive turbulence in a bounded domain. Magnetic geometry and boundary effects break symmetry and *total* momentum conservation, so that a net toroidal flow develops. Two heat engines, a car and a tokamak, are compared in table 2. The engine process effectively converts radial inhomogeneity into parallel flow via symmetry-breaking induced non-diffusive component of the Reynolds stress $\langle \tilde{v}_r \tilde{v}_\parallel \rangle$, as shown in figure 4. The heat engine paradigm was developed to explain the formation of geophysical flows [42] and the solar differential rotation [43] (table 3). Both are prime examples of flows produced by heat flux-driven turbulence.

Here, we summarize the heat engine model, derived from the consideration of fluctuation entropy balance. This

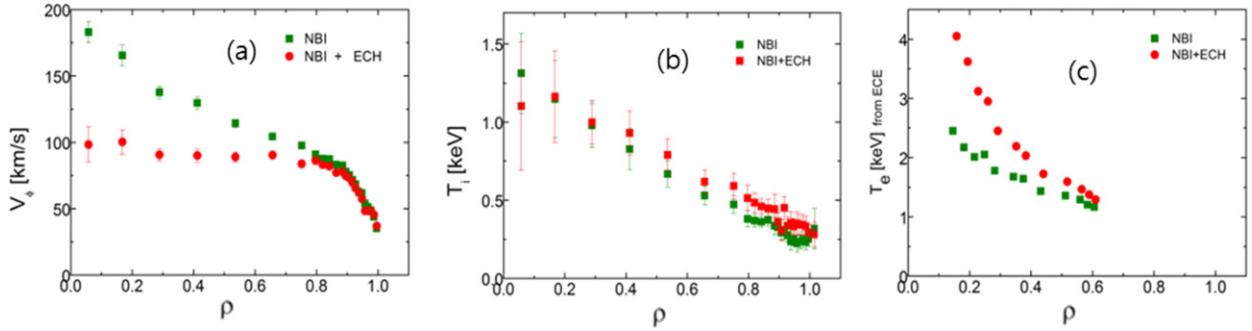

Figure 3. CES profiles from KSTAR co-NBI H-mode + ECH experiments [36]. Note that injection of 400 kW of ECH on axis into 1.2 MW co-NBI plasmas tends to flatten the $\langle v_\phi \rangle$ profile, sharply peak the $\langle T_e(r) \rangle$ profile and leave the $\langle T_i(r) \rangle$ profile almost unchanged.

Table 2. Table comparing two heat engines, a car and intrinsic rotation in tokamaks.

	Car	Intrinsic rotation
Fuel	Gas	Heating $\Rightarrow \nabla T$
Conversion	Burn	∇T driven DW turbulence
Work	Cylinder/Cam	Residual stress
		symmetry breaking $\rightarrow$ direction
Result	Wheel rotation	Flow

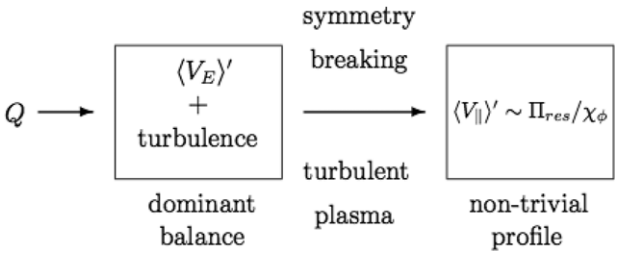

Figure 4. Turbulent plasma and flow generation.

discussion is necessarily short—readers are referred to the original literature for details [7]. Fluctuation entropy is an especially convenient framework within which to consider turbulent relaxation, since it is closely related to the phase space density fluctuation intensity. For ITG turbulence, the kinetic fluctuation entropy density $\langle \delta f^2 \rangle / (2\langle f \rangle)$ is

$$\partial_t \left\langle \frac{\delta f^2}{2\langle f \rangle} \right\rangle + \frac{1}{r}\partial_r \left(r \left\langle \tilde{V}_r \frac{\delta f^2}{2\langle f \rangle} \right\rangle \right) - \frac{\langle \delta f C(\delta f) \rangle}{\langle f \rangle} = -\langle \tilde{v}_r \delta f \rangle \frac{\langle f \rangle'}{\langle f \rangle} - \frac{|e|}{m_i} \langle \tilde{E}_\parallel \delta f \rangle \frac{1}{\langle f \rangle} \frac{\partial \langle f \rangle}{\partial v_\parallel} \quad (3)$$

so the local fluctuation entropy balance is

$$\partial_t \int \mathrm{d}\Gamma \frac{\langle \delta f^2 \rangle}{2\langle f \rangle} = \int \mathrm{d}^3 x (\mathcal{P} - \mathcal{D}). \quad (4)$$

Here, $\int \mathrm{d}\Gamma$ is an integral over phase space, $\mathcal{P}$ is production and $\mathcal{D}$ is dissipation. Production P is given by

$$\mathcal{P} = \int \mathrm{d}^3 v \left(-\langle \tilde{v}_r \delta f \rangle \frac{\langle f \rangle'}{\langle f \rangle} - \frac{|e|}{m_i} \langle \tilde{E}_\parallel \delta f \rangle \frac{1}{\langle f \rangle} \frac{\partial \langle f \rangle}{\partial v_\parallel} \right) \cong n\chi_i \left(\frac{\nabla T}{T} \right)^2 - nK \left(\frac{\langle V_E \rangle'}{v_{thi}} \right)^2 + n\chi_\phi \left(\frac{\langle V_\parallel \rangle'}{v_{thi}} \right)^2 - n \frac{\Pi_{r\parallel}^{res\,2}}{v_{thi}^2 \chi_\phi}. \quad (5)$$

The first term in $\mathcal{P}$ is thermal relaxation, the second term is due to $\boldsymbol{E} \times \boldsymbol{B}$ flow generation, the third is turbulent viscous heating due to $\langle V_\parallel \rangle'$ relaxation, and the fourth is related to intrinsic rotation generation by $\Pi_{r\parallel}^{res}$. Note terms 1,3 are *positive definite*, reflecting *entropy production by relaxation*, while terms 2, 4 are *negative definite*, reflecting *entropy destruction by flow generation*. The zonal shear is controlled by the balance of Reynolds force versus drag, so the system has the familiar 'predator-prey' structure. This formulation suggests a natural definition of engine efficiency $e \equiv \int \mathrm{d}^3 x P_{flow}^d / \int \mathrm{d}^3 x P_{total}^p$, as the ratio of entropy *destruction* by toroidal flow generation to total entropy *production* by relaxation. Detailed calculations [7] give $\langle V_\parallel \rangle' \cong -(\rho_*/2)(\chi_i/\chi_\phi)(L_s/c_s)((\nabla T)/T)^2 v_{thi}^2$. For no-slip boundary conditions, it follows that: $\langle V_\parallel \rangle / v_{thi} \cong (\rho_*/2)(\chi_i/\chi_\phi)(L_s/L_T)\sqrt{T_i/T_e}$ and $e \cong \rho_*^2 (q^2/\hat{s}^2)(R/L_T)^2$. The sign and magnitude of the predicted $\langle V_\parallel \rangle$ agree with C-Mod results [8]. Note that $\langle V_\parallel \rangle$ scales with L_T^{-1}, in accord with experiments, and taking $1/L_T \sim \Delta W_p$ and $L_s \sim q \sim B_\theta^{-1}$ recovers the basic trend of the Rice scaling, i.e. $\Delta v_\phi \sim \Delta W_p / I_p$. Similarly, the $\langle V_\parallel \rangle \sim \nabla T / B_\theta$ scaling of Ida *et al* [44] is also recovered. Note also the explicit, direct ρ_* scaling originates from the underlying turbulence model and symmetry-breaking mechanism. Zonal shear intensity at saturation is $\langle V_E' \rangle^2 = (\chi_i/K) v_{thi}^2 / L_T^2$. Here K is quadratic in fluctuation amplitude and originates from the perpendicular Reynolds stress. The heat engine efficiency is $e \sim M_i^2$, where M_i is the toroidal Mach number, so $e \sim .01 \rightarrow .1$ for $M_i \sim .1 \rightarrow .3$. e scales according to $e \sim \rho_*^2 (q^2/\hat{s}^2) R^2 / L_T^2$, and $e \sim \langle (k_\parallel / k_\theta)^2 \rangle$. Note that apart from the ρ_* dependence, the scaling behaviour of e is similar to the Rice scaling. Of course, for CTEM turbulence, ∇n and ∇T_e replace ∇T_i as the relevant thermodynamic forces, which will enter the scaling. Figure 5 shows a plot of intrinsic torque versus ∇T_i for ITG turbulence [45], while figure 6 shows the corresponding intrinsic torque versus ∇T_e and ∇n for CTEM turbulence [46]. Note that in all cases, the residual stress scales directly with the driving gradient (i.e. the relevant thermodynamic force). Of course the ρ_* scaling is a concern for possible extrapolations to ITER, though ρ_* scaling is not manifested in empirical studies of intrinsic rotation scaling [4].

The main intrinsic limitation of this approach is its local formulation and simplified boundary condition. In particular, fluctuation entropy transport (i.e. turbulence avalanching and spreading) and dynamics of heat flux relaxation [47] can significantly modify the dependences. Research in these issues is ongoing. Non-locality and intrinsic torque are discussed in section 4.5.

Table 3. Comparison of differential rotation in the sun and intrinsic rotation in tokamak.

	Sun	Tokamak
Heat source	Fusion reaction in the core	Heat deposition
Turbulence source	∇T	∇T
threshold	Schwarzschild Criteria $\frac{1}{T}\left\|\frac{dT}{dz}\right\| > (\gamma-1)\frac{1}{\rho}\left\|\frac{d\rho}{dz}\right\|$	ITG $R/L_T > R/L_{T,c}$
Turbulence	Convective turbulence	Drift-ITG turbulence
Symmetry breaking	Rotation, β Stratification	Velocity shear, $\langle V_E\rangle'$ Intensity gradient, $I(x)$, ...
Resultant flow	Polar differential rotation $v_\phi(\theta)$	Intrinsic rotation $v_\parallel(r)$
Boundary condition	Momentum loss to solar wind	Edge stresses, SOL flow effects, neutral drag

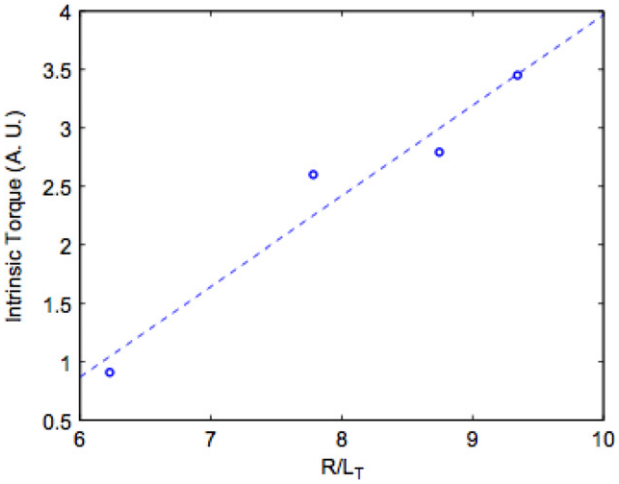

Figure 5. Intrinsic torque versus ITG as measured by simulations of ITG turbulence [45].

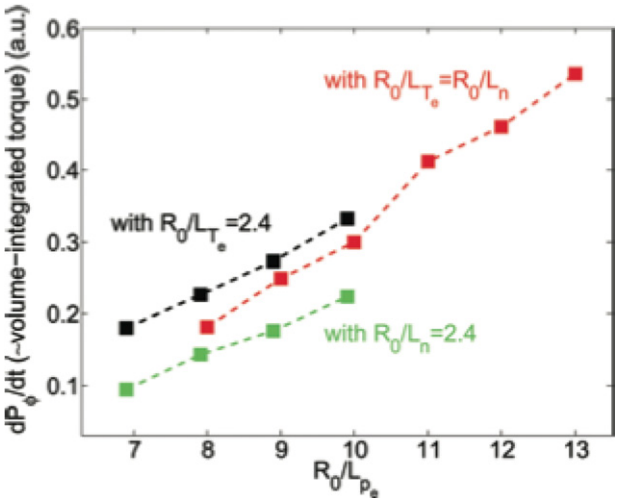

Figure 6. Intrinsic torque versus electron pressure (electron temperature and density) gradient as measured by simulations of CTEM turbulence [46].

4. Theory of intrinsic torque

This section surveys the physics of the most relevant symmetry-breaking mechanisms. This survey is necessarily limited—other mechanisms do exist. We focus on the most important physical properties of the mechanisms of interest. The reader concerned with detailed calculations should consult the primary literature. The discussion is summarized in table 4.

The net residual stress $\Pi^R_{r\phi}$ is given by

$$\Pi^R_{r\phi} = nm_i\left[\langle \tilde{v}_{E,r}\tilde{v}_\parallel\rangle^R + \left\langle \frac{c}{B}\tilde{E}_r\frac{c}{B}\tilde{E}_\parallel\right\rangle - \frac{B_\theta}{B_T}\langle \tilde{v}_{E,r}\tilde{v}_\theta\rangle\right]. \quad (6)$$

Each term represents a specific process and is determined by a specific spectrally weighted correlator of two wavenumber components. This correlator contains the essence of the symmetry-breaking physics, much the same way the turbulence helicity contains the essence of reflectional symmetry breaking, which is crucial to the mean field theory of the turbulent magnetic dynamo [48]. Indeed, symmetry breaking is well to be central to large scale flow generation in turbulent neutral fluids [49]. The first term is the residual part of the parallel Reynolds stress, due to radial transport of parallel velocity, which is determined by the spectral correlator $\langle k_\theta k_\parallel\rangle$. Here the bracket refers to a spectral average, i.e. $\langle k_\theta k_\parallel\rangle = \sum_k k_\theta k_\parallel|\tilde{\phi}_k|^2/\sum_k|\tilde{\phi}_k|^2$. The second term is the polarization stress, which actually originates from parallel acceleration of guiding centres by the gyrokinetic polarization charge [50]. The key correlator here is $\langle k_r k_\parallel\rangle$. The third term is due to the toroidal projection of perpendicular forces, or, equivalently, the $\langle \boldsymbol{J}\rangle_{\text{radial}} \times \boldsymbol{B}_\theta$ force induced by a radial flux of polarization charge. The relevant correlator is $\langle k_\theta k_r\rangle$, familiar from the perpendicular Reynolds stress which drives zonal flow (ZF) [51], etc.

The residual part of the parallel Reynolds stress, determined by the $\langle k_\theta k_\parallel\rangle$ correlator, is effectively set by the spatial structure of the spectrum $|\tilde{\phi}_k(r)|^2$, since radial structure couples to parallel variation via $k_\parallel = k_\parallel(r)$, and since the sum over modes implies a spatial integration. Hence, the $\langle k_\theta k_\parallel\rangle$ correlator is sensitive to asymmetries. The first of these is due to spatial spectral shifts as shown in figure 7. Sheared flows (i.e. $\langle V_E\rangle'$) tend to shift modes off resonant surfaces [52, 53], producing a skewed intensity profile, which in turn gives a finite spectrally averaged value of $\langle k_\parallel\rangle$. This produces an imbalance in acoustic wave populations with $\pm k_\parallel$, and so gives a finite $\langle k_\theta k_\parallel\rangle$. A spectral intensity shift is thus the signature of $k_\parallel$ symmetry breaking by $\boldsymbol{E}\times\boldsymbol{B}$ shear. In ballooning space [32], $\boldsymbol{E}\times\boldsymbol{B}$ shear produces an eddy shift and tilt. Note that the shift

Table 4. Physics of symmetry breaking mechanisms.

Relevant stress and mechanism	Spatial structure	Key physics	Macro implication
$\langle \tilde{v}_r \tilde{v}_\parallel \rangle$, $\langle v_E \rangle'$ (Electric field shear)	$k_\parallel$ from spectrum *shift* (config.) or *eddy tilt* (ballooning)	Centroid shift induces mean $\langle k_\parallel \rangle$ from parallel acoustic wave asymmetry	$\pi_{res} \sim \langle v_E \rangle'$. Intrinsic torque peaked at barriers, steep gradients π_{res} can flip with mode change
$\langle \tilde{v}_r \tilde{v}_\parallel \rangle$, I' (Intensity gradient) ($I \equiv$ intensity)	$k_\parallel$ from spectra *dispersion* due I'	Spectral dispersion from intensity gradient. Linked to $\perp$ Reyn. stress, also	$\pi_{res} \sim I'$. relevant to barriers but also for more general inhomogeneity. Can change with mode change. Ultimately tied to temp. profile curv.
Stress from polarization acceleration $\langle \tilde{E}_\parallel \nabla_\perp^2 \tilde{\phi} \rangle$	$\langle k_r k_\parallel \lvert \phi_k \rvert^2 \rangle$ stress due radial + parallel propagation, $(r, \parallel)$ tilting	Guiding centre stress from acceleration due polarization charge $\langle k_r k_\parallel \rangle \neq 0$ needed	As yet unclear. Merits further study. Linked to mode radial group velocity v_{gr} and can flip direction
Stress from $\partial_r \langle \tilde{v}_r \tilde{v}_\perp \rangle \rightarrow \langle J_r \rangle \rightarrow B_\theta \langle J_r \rangle$ $\rightarrow$ toroidal torque	(r, θ) tilting, as for ZF Same physics for ZF	$\boldsymbol{J} \times \boldsymbol{B}$ torque originating from polarization flux $I' \neq 0$, $\langle k_r k_\theta \rangle \neq 0$ needed	$\sim$ universal mechanism, closely related to ZF, tied to I' and I_k structure. Flips with v_{gr}. Merits more study.

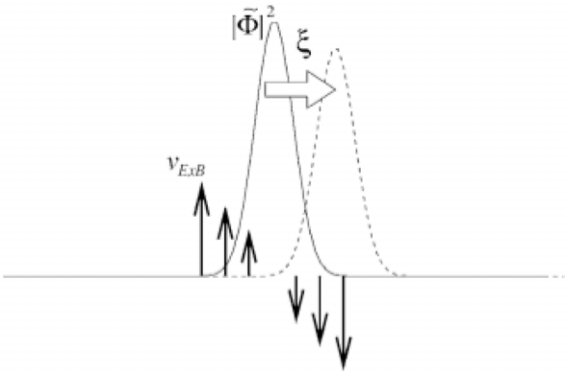

Figure 7. Symmetry breaking by $\langle V_E \rangle'$-induced spectral shift [53]. Finite $\langle V_E \rangle'$ renders the spectral centroid non-zero, and so yields $\langle k_\parallel \rangle$.

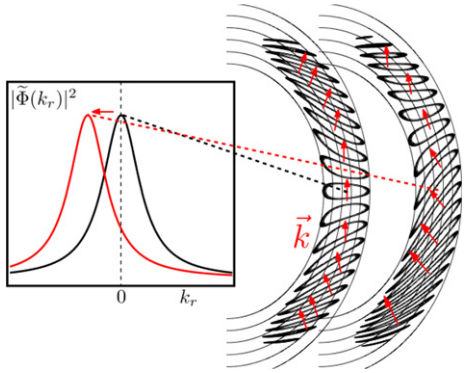

Figure 8. Shifted spectrum in real space and net eddy tilt in ballooning space. Note a Fourier transform directly relates the 'tilted' spectrum in ballooning space to the shifted spectrum in configuration space.

is necessarily proportional to $\langle V_E \rangle'$, and cannot be so large that the underlying shear turns the underlying instability off. The correspondence between the configuration and the ballooning space manifestations of shear flow induced symmetry breaking is shown in figure 8. Note the connection between mean $k_\parallel$ (i.e. $\langle k_\parallel \rangle$) and net eddy tilt. Clearly the real space and ballooning space approaches are equivalent.

A second, *equally important* mechanism for symmetry breaking in $\langle k_\theta k_\parallel \rangle$ is due to spatial spectral dispersion, with finite intensity *gradient* I' [54, 55]. This mechanism does not require a spectral *shift*. Rather, the requisite asymmetry is produced by the spatial profile of intensity. The origin of this effect can be seen from

$$\langle k_\theta k_\parallel |\tilde{\phi}_k|^2 \rangle \simeq \left\langle k_y^2 \frac{(r - r_0)}{L_s} \left\{ |\tilde{\phi}_k|^2 + (r - r_0) \frac{\partial}{\partial r} |\phi_k(\tilde{r}_0)|^2 + \cdots \right\} \right\rangle \approx \left\langle k_y^2 \frac{(r - r_0)^2}{L_s} \frac{\partial}{\partial r} |\tilde{\phi}_k|^2 \right\rangle. \quad (7)$$

Figure 9 gives an instructive heuristic sketch related to this mechanism. Note that intensity gradients will surely be steep at the boundary between regions with different confinement properties (for example, at the 'corners', which bound transport barriers where profile curvature is large). Thus, strong intensity gradients will occur near regions with large changes in $\langle V_E \rangle'$. However, one can expect an intensity gradient in

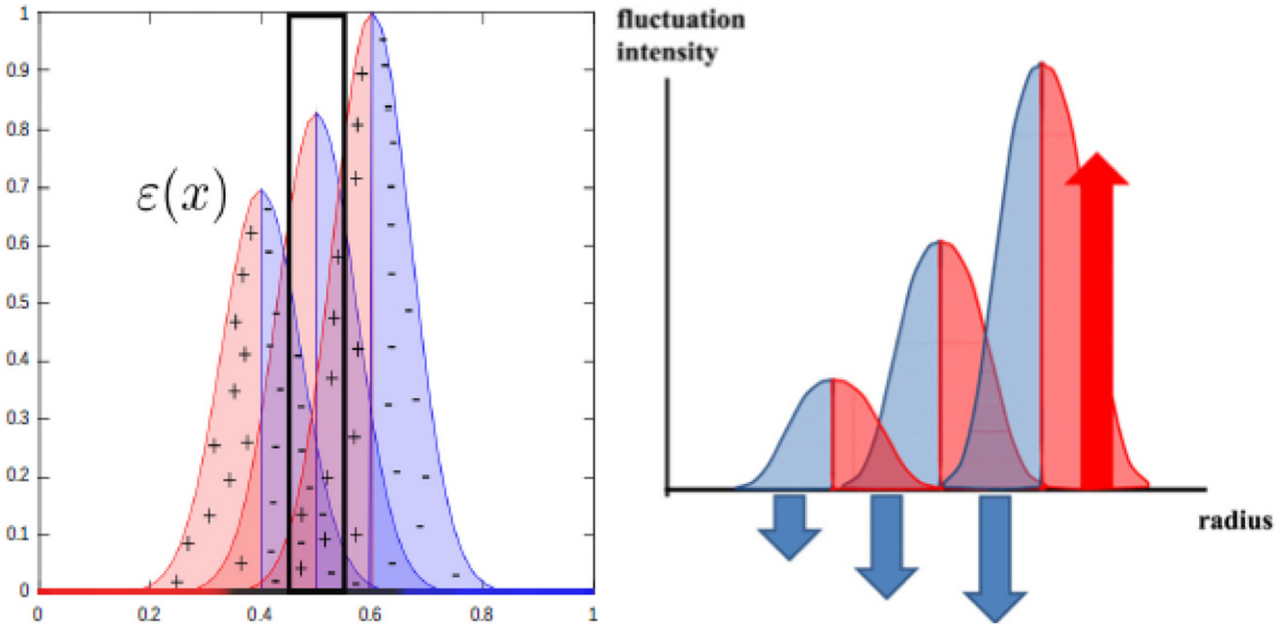

Figure 9. Symmetry breaking by I'-induced spectral dispersion [54, 55].

any region of significant temperature profile curvature. This may easily be seen by considering the condition of constant total heat flux, taken as diffusive for simplicity. Then, for $Q = -(\chi_T + \chi_{neo})\partial_r\langle T\rangle$,

$$Q' \cong 0 \tag{8}$$

requires

$$\frac{1}{\chi_T}\partial_r\chi_T \cong -\frac{1}{\partial_r\langle T\rangle}\partial_r^2\langle T\rangle - \frac{1}{\chi_T}\frac{\partial\chi_{neo}}{\partial r}. \tag{9}$$

Here χ_T is the turbulent heat diffusivity. For simplicity, we also assume $\chi_T > \chi_{neo}$. Thus, noting $\partial_r\chi_T/\chi_T \sim \partial_r I/I$, we find

$$\frac{\partial_r I}{I} \cong -\frac{\partial_r^2\langle T\rangle}{\partial_r\langle T\rangle}, \tag{10}$$

i.e. temperature profile *curvature* is seen to be closely related to the fluctuation intensity gradient. Notice that it is profile curvature, rather than profile shear, which ultimately determines the residual stress and intrinsic torque nominally produced by fluctuation intensity gradients. Also note that both intensity gradient and electric field shear mechanisms ultimately depend heavily on profile curvature, the latter via $\{1/(en)\}\partial_r^2\langle p_i\rangle$, from radial force balance. We see that the intensity gradient mechanism is, in some sense, more general than the $E \times B$ shear mechanism.

Given the complexity of symmetry-breaking physics, it is natural to seek to test the theory via numerical simulation. With the possible exception of full f, flux-driven studies, gyrokinetic simulations have somewhat limited capacity to investigate intrinsic rotation phenomena. Boundary conditions—both for flow and for heat—remain especially thorny issues. Simulations can, however, investigate symmetry-breaking mechanisms. One study of flux-driven ITG turbulence [45] compared the correlation between residual stress and intrinsic torque, with parallel symmetry-breaking mechanisms due to $\langle V_E\rangle'$ and I' (intensity gradient). Figure 10 shows the correlations of residual stress and intrinsic torque with the candidate mechanisms. The degrees of correlation are quite comparable, with the intensity gradient mechanism exhibiting the same level of correlation as the usually invoked $\langle V_E\rangle'$. Interestingly, correlations with intrinsic torque are stronger than with residual stress.

Another contribution to the residual stress is the second term in equation (6), which actually originates from parallel acceleration of guiding centres by GK polarization charge $\sim\langle\tilde{E}_\parallel\nabla_\perp^2\tilde{\phi}\rangle$ [50]. Ignoring other co-existing symmetry breaking mechanisms, we can re-write this acceleration effect as the divergence of a stress $\Pi^R_{r\phi} \sim \langle\tilde{E}_\parallel\partial_r\tilde{\phi}\rangle$. The key correlator for this stress is $\langle k_\parallel k_r\rangle$. Interestingly, this correlator is typically non-zero for *any* out-going wave, i.e. with the structure $k_\parallel \sim k_\theta x/L_s$, while $k_r = -\mu_k x$ so $\langle k_\parallel k_r\rangle \sim \langle(k_\theta\mu_k)x^2/L_s\rangle \neq 0$. There is no need to invoke additional 'symmetry breaking'. In this sense, the polarization stress is a *universal* contribution to Π^R, which is likely to be present in *all* confinement and transport regimes. We comment that Π^R_{pol} merits more attention than it has received to date.

A fourth mechanism, corresponding to the third term on the right-hand side (RHS) of equation (6) follows from the *toroidal projection* of the *perpendicular Reynolds stress* [56], $\langle\tilde{v}_r\tilde{v}_\perp\rangle$. Since the stress $\langle\tilde{v}_r\tilde{v}_\perp\rangle$ is fundamentally rooted in wave propagation and necessarily depends upon radial group velocity v_{gr} [51], we refer to this as the wave residual stress Π^R_w. The way by which Π^R_w drives toroidal rotation may be thought of either as a result of a non-zero divergence of a stress $(\sim(B_\theta/B_T)\langle\tilde{v}_r\tilde{v}_\perp\rangle)$, or as a toroidal torque $\langle J_r\rangle B_\theta/c$. The two approaches are precisely equivalent. Here $\langle J_r\rangle$ is the radial current produced by the radial flux of polarization charge $(\langle J_r\rangle \sim B_\theta\langle\tilde{v}_r\rho_s^2\nabla_\perp^2\tilde{\phi}\rangle/B_0 \sim (B_\theta/B_0)\partial_r\langle\tilde{v}_r\tilde{v}_\theta\rangle$, by the Taylor identity [57, 58]). Now, the Reynolds stress is more conveniently calculated by using wave kinetics and modulation theory. The result, which follows from a standard calculation

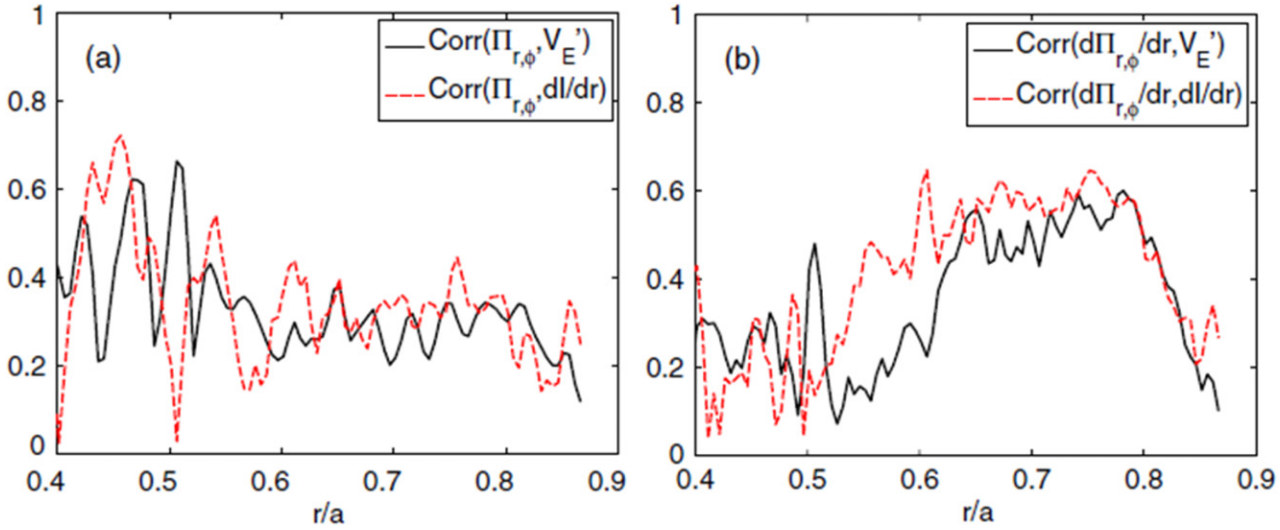

Figure 10. Comparison of symmetry-breaking mechanisms related to $E \times B$ shear $\langle V \rangle'$ and intensity gradient I' [45]. The levels of correlation with $\Pi_{r\phi}$ are comparable.

[51], is

$$\Pi^{\mathrm{R}}_{\mathrm{wave}} = \sum_{\boldsymbol{k}} \left\{ - D_w \frac{\partial}{\partial r}(k_\theta \langle N \rangle) - \frac{k_\theta^2 \rho_s^2 \tau_{c\boldsymbol{k}}}{(1 + k_\perp^2 \rho_s^2)^2} k_r \frac{\partial}{\partial k_r} \langle \Omega \rangle \langle V_E \rangle' \right\}, \tag{11}$$

where $D_w = v_{\mathrm{gr}}^2 \tau_{c\boldsymbol{k}}$ and $\langle \Omega \rangle$ is the wave enstrophy density, proportional to the wave action density. Note that the first term is effectively an intensity gradient contribution and is determined by the radial profile of wave poloidal momentum density itself, $\sim k_\theta \langle N(\boldsymbol{k}, \boldsymbol{x}) \rangle$. $\tau_{c\boldsymbol{k}}$ is the wave-flow correlation time. The first term corresponds to spatial diffusion of wave momentum density, due to the random walk (in the space) of interacting wave packets. D_w is the spatial diffusion coefficient for this walk. The second term is familiar from ZF theory [51], and represents growth by ZF amplification. Equation (11) states that both radial position and radial wavenumber gradients of the spectral density contribute to driving the mean stress and intrinsic flow. Physically speaking, the second term describes how shear-induced eddy tilting produces a stress, while the first describes how a gradient in wave momentum density can drive a flow. Interestingly, this mechanism is quite robust, and appears stronger than conventionally invoked effects derived from $\langle \tilde{v}_r \tilde{v}_\parallel \rangle$, since usually $|(B_\theta/B_0)\langle \tilde{v}_r \tilde{v}_\perp \rangle| > |\langle \tilde{v}_r \tilde{v}_\parallel \rangle|$. Note also that the wave stress does not require any special symmetry-breaking effect, apart from the existence of a non-zero spectral gradient in either $\boldsymbol{x}$ or $\boldsymbol{k}$. Thus, the force induced by the toroidal projection of the $\langle \tilde{v}_r \tilde{v}_\perp \rangle$ intrinsic torque stress surely merits more attention as a drive for intrinsic rotation.

We emphasize here that while this list includes the most important and most frequently invoked symmetry-breaking mechanisms, there are many others. The constraints on this rather short OV paper preclude an exhaustive discussion. The reader is referred to other OV papers and to the original literature for additional details.

4.1. Gyrokinetic formulation of intrinsic torque

The approach of the previous section was intuitive and heuristic. There, we sought to motivate and present the key physics of the mechanisms which underpin intrinsic torque. In this complementary section, we present a gyrokinetic formulation of intrinsic torque. The approach is systematic and deductive, and the aim is to indicate how and where the effects discussed in section 4.1 originate in the gyrokinetic equation.

For an electrostatic axisymmetric equilibrium, the expression for the evolution of toroidal canonical momentum $p_\varphi \equiv m_s R b_\varphi v_\parallel - q_s \psi/c$ may be written as [59]

$$\frac{\partial}{\partial t}\left\langle p_\varphi B_\parallel^* F_s \right\rangle + \frac{1}{V'}\frac{\partial}{\partial \psi} V' \left\langle p_\varphi B_\parallel^* F_s \dot{\boldsymbol{X}} \cdot \nabla \psi \right\rangle + \frac{\partial}{\partial v_\parallel}\left\langle p_\varphi B_\parallel^* F_s \dot{V}_\parallel \right\rangle = -\left\langle q_s B_\parallel^* \delta F_s \frac{\partial \delta \phi}{\partial \varphi} \right\rangle, \tag{12}$$

where we have taken the limit of cold ions, so that finite Larmor radius effects may be neglected. Here $\boldsymbol{B}^* = \boldsymbol{B} + (m_i c/e)\nabla \times (v_\parallel \boldsymbol{b})$. This limit was taken for reasons of simplicity and may be easily relaxed (see [50, 60, 61] for treatments of finite Larmor radius terms). Integrating equation (12) over velocity space, and summing over particle species, yields

$$\frac{\partial}{\partial t}\left\langle \sum_s \int \mathrm{d}^3 v p_\varphi F_s \right\rangle + \frac{1}{V'}\frac{\partial}{\partial \psi} V' \left\langle \sum_s \int \mathrm{d}^3 v p_\varphi F_s \dot{\boldsymbol{X}} \right\rangle = -\left\langle \sum_s q_s \int \mathrm{d}^3 v \delta F_s \frac{\partial \delta \phi}{\partial \varphi} \right\rangle, \tag{13}$$

where the velocity space volume element is given by $\mathrm{d}^3 v \equiv 2\pi\, \mathrm{d}\mu\, \mathrm{d}v_\parallel B_\parallel^*$. Equation (13) indicates that toroidal canonical momentum is conserved up to the breaking of axisymmetry by the fluctuating electrostatic field. This expression may be transformed into an expression for the angular momentum $L_\varphi \equiv m_s R b_\varphi v_\parallel$ by multiplying the particle conservation equation by $q_s \psi/c$ and summing the result with equation (13),

yielding

$$\frac{\partial}{\partial t}\left\langle \sum_s \int \mathrm{d}^3 v L_\varphi F_s \right\rangle + \frac{1}{V'}\frac{\partial}{\partial \psi} V' \left\langle \mathbf{\Pi}_\varphi \cdot \nabla \psi \right\rangle = \left\langle R \delta q^{\mathrm{pol}} \delta E_\varphi \right\rangle + R \frac{\langle J_r \rangle B_\theta}{c}. \tag{14}$$

Here we have defined the polarization charge and radial current by

$$\delta q^{\mathrm{pol}} = \sum_s q_s \int \mathrm{d}^3 v \delta F_s, \qquad J_r = \sum_s q_s \int \mathrm{d}^3 v F_s \dot{\boldsymbol{X}} \cdot \hat{\boldsymbol{e}}_r,$$

the flux of angular momentum is given by

$$\mathbf{\Pi}_\varphi \equiv \sum_s \int \mathrm{d}^3 v L_\varphi F_s \dot{\boldsymbol{X}}. \tag{15}$$

and we have defined the radial unit vector by $\hat{\boldsymbol{e}}_r \equiv \nabla\psi/|\nabla\psi|$ where $|\nabla\psi| = B_\theta R$. Equation (14) suggests that the plasma may be accelerated by the radial flux of toroidal momentum, the application of a $J \times B$ torque, or through the toroidal acceleration of the plasma by the fluctuating electric field.

The $J \times B$ torque appearing on the rhs of equation (14) can be further constrained by considering the gyrokinetic Poisson equation. Namely, taking the time derivative of the flux surface averaged linearized gyrokinetic Poisson equation, yields

$$\left\langle \nabla_\perp \cdot \left(\epsilon_\perp \frac{\partial}{\partial t} \nabla_\perp \phi \right) \right\rangle = -4\pi \left\langle \sum_s q_s \int \mathrm{d}^3 v \frac{\partial F_s}{\partial t} \right\rangle = 4\pi \left\langle \nabla_\perp \cdot \sum_s q_s \int \mathrm{d}^3 v F_s \dot{\boldsymbol{X}} \right\rangle, \tag{16}$$

where $\epsilon_\perp \equiv c^2/v_{\mathrm{A}}^2$ and we have utilized the conservative form of the gyrokinetic Vlasov equation. After performing an integration over the radial direction, the mean radial current may be shown to be constrained by the temporal variation of the mean radial electric field, i.e.

$$-\frac{\epsilon_\perp}{4\pi}\frac{\partial}{\partial t}\langle E_r \rangle = \langle J_r \rangle. \tag{17}$$

The $J \times B$ torque on the rhs of equation (14) may then be rewritten as

$$\frac{\langle J_r \rangle B_\theta}{c} = -\frac{\epsilon_\perp}{4\pi}\frac{\partial}{\partial t}\frac{\langle E_r \rangle B_\theta}{c}, \tag{18}$$

which may be recognized as the rate of change of the mean toroidal field momentum. Similarly, utilizing the gyrokinetic Poisson equation, the toroidal acceleration term may be rewritten as

$$\left\langle R \delta q^{\mathrm{pol}} \delta E_\varphi \right\rangle = \frac{1}{V'}\frac{\partial}{\partial \psi} V' \left\langle n_0 m_{\mathrm{i}} \frac{c^2}{B^2} \nabla_\perp \delta\phi \cdot \nabla\psi \frac{\partial \delta\phi}{\partial \varphi} \right\rangle, \tag{19}$$

where we have exploited the axisymmetry of the magnetic equilibrium. Hence, from equations (17), (19) and (14), the evolution of the total toroidal momentum is described by

$$\frac{\partial}{\partial t}\left(\left\langle L_\varphi^{\mathrm{mech}} \right\rangle + \left\langle L_\varphi^{\mathrm{field}} \right\rangle \right) + \frac{1}{V'}\frac{\partial}{\partial \psi} V' \left[\left\langle \mathbf{\Pi}_\varphi \cdot \nabla\psi \right\rangle + \left\langle \mathbf{\Pi}_{\mathrm{pol}} \cdot \nabla\psi \right\rangle \right] = 0, \tag{20}$$

where we have defined the flux

$$\mathbf{\Pi}_{\mathrm{pol}} \equiv -n_0 m_{\mathrm{i}} \frac{c^2}{B^2} \nabla_\perp \delta\phi \frac{\partial \delta\phi}{\partial \varphi}. \tag{21}$$

Here the mechanical and field momenta are defined by

$$L_\varphi^{mech} \equiv \sum_s \int \mathrm{d}^3 v L_\varphi F_s, \qquad L_\varphi^{\mathrm{field}} \equiv R \frac{\epsilon_\perp}{4\pi} \frac{\langle E_r \rangle B_\theta}{c}. \tag{22}$$

For practical purposes, it is often convenient to decompose the polarization stress into perpendicular and parallel components, i.e.

$$\left\langle \mathbf{\Pi}_{\mathrm{pol}} \cdot \hat{\boldsymbol{e}}_r \right\rangle = -n_0 m_{\mathrm{i}} \left\langle R \frac{B_\theta}{B} \delta u_y^{EB} \delta u_r^{EB} \right\rangle - n_0 m_{\mathrm{i}} \left\langle R \frac{B_\varphi}{B} \frac{c^2}{B^2} \delta E_r \delta E_\parallel \right\rangle.$$

Here the first contribution can be recognized as the toroidal projection of the perpendicular Reynolds stress, whereas the second contribution represents the toroidal projection of a parallel stress associated with the acceleration of gyrokinetic polarization charge. The second contribution corresponds to the parallel Reynolds stress $\langle \tilde{v}_r \tilde{v}_\parallel \rangle$ discussed in section 4.1, while the second corresponds to $(B_\theta/B_{\mathrm{T}})\langle \tilde{v}_r \tilde{v}_\perp \rangle$, also discussed there.

4.2. Alternative formulation by wave kinetics

In this section, we survey an alternative formulation of the physics of residual stress [31]. The formulation here is based on the same idea as the energy conservation balance in basic quasi-linear theory. There, an appealing picture of an energy balance between *resonant particles* and *waves* emerges [62, 63]. In that spirit, here we calculate the net momentum flux and residual stress by a decomposition into *resonant ion momentum flux* and *wave momentum flux*. The wave momentum flux is most conveniently calculated by a type of Chapman–Enskog expansion of the wave kinetic response, using the wave kinetic equation. The utility of this approach is that it is rather systematic, yields a unified structure within which to examine trade-offs and competition, and gives an alternative perspective to the approach presented in section 4.1. In particular, it elucidates the important links between wave propagation, momentum transport, and intrinsic torque.

Here we briefly summarize the calculation and discuss the physics of the principal results. We limit this discussion to wave momentum (i.e. equivalent to non-resonant particle momentum), as *most ions which support drift-ITG turbulence are non-resonant*. Resonant particle momentum transport is discussed in detail in [31]. The radial flux of parallel wave momentum (which corresponds to the radial flux of non-resonant particle parallel momentum) is given directly by $\sum_{\boldsymbol{k}} k_\parallel v_{gr} N(\boldsymbol{k})$. This quantity is most expeditiously calculated using a linear response approximation for the wave population (i.e. action) density $N(\boldsymbol{k}, x)$, in the spirit of a Chapman–Enskog expansion (see [31]). This yields the response of the gas of waves to thermodynamic forces. Omitting details, the result is:

$$\Pi_{r\parallel}^{\mathrm{R}} \simeq \int \mathrm{d}\boldsymbol{k} k_\parallel \left\{ -\tau_{\mathrm{c},k} v_{\mathrm{gr}}^2 \frac{\partial}{\partial r}\langle N \rangle + \tau_{\mathrm{c},k} v_{\mathrm{gr}} k_\theta \langle V_E \rangle' \frac{\partial}{\partial k_r}\langle N \rangle \right\}. \tag{23}$$

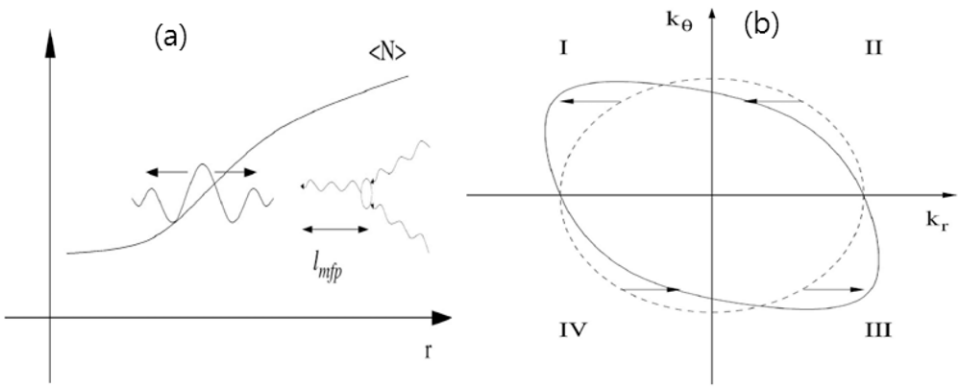

Figure 11. Drives of wave residual stress [31]. (*a*) shows the effect of spectral inhomogeneity (intensity gradient) and (*b*) shows the effect of shearing and shear-induced tilt.

The first term on the rhs accounts for spatial transport of parallel wave momentum by scattering wave packets, which leads to wave momentum density diffusion. It is effectively an intensity gradient effect. As $\partial\langle N\rangle/\partial r > 0$ (i.e. since fluctuation intensity increases with radius), the effect generates an inward flux of positive wave momentum ($k_\parallel > 0$) and/or an outward flux of negative wave momentum ($k_\parallel < 0$). Any intensity gradient then necessarily *must* produce a finite flux and residual stress. This effect is particularly strong at the edge, where intensity gradients are steep. The second term accounts for refraction induced wave quanta imbalance. This is evidently important in regions of strong $\langle V_E\rangle'$, such as for steep ∇P, relevant to barriers. It is important to notice that dependence on the propagation direction of the underlying mode enters via the $v_{\rm gr}$ factor, which can flip sign when ITG $\rightarrow$ TEM. The physics of $\Pi^{\rm R}_{r\parallel}$ is schematically shown in figure 11. The $\langle V_E\rangle'$ dependence follows from a refraction induced change in wave population (and momentum) density due to shearing.

An interesting observation concerning the wave radiation stress given in equation (23) is that it clearly can support multiple types of transport bifurcations, implying multiple states of toroidal momentum transport. In particular, a glance at the 2nd term suggests that $\Pi^{\rm R}_{r\parallel}$ associated with this contribution ($\sim v_{\rm gr}\langle V_E\rangle'$) can change either by: (a) a change in $\langle V_E\rangle'$ at constant $v_{\rm gr}$ or (b) a change in $v_{\rm gr}$ at constant $\langle V_E\rangle'$. The former corresponds to the L $\rightarrow$ H spin-up, or ITB formation, where $\langle V_E\rangle'$ increases dramatically. Note that changes in fluctuation intensity are largely irrelevant, since for intrinsic rotation, $\langle v_\phi\rangle' \sim \Pi_{\rm resit}/\chi_\phi$, so fluctuation amplitude approximately cancels out. Of course, *some* residual turbulence in the barrier is required to sustain $\Pi^{\rm res}$. The second type of momentum transport bifurcation corresponds to *reversals*, where a change in sign of $v_{\rm gr}$, and thus $\Pi^{\rm R}$, can result from a $v_{*\rm e} \leftrightarrow v_{*\rm i}$ flip (i.e. TEM $\leftrightarrow$ ITG). Note that in the former case, the momentum transport bifurcation is closely linked to a confinement bifurcation (as $\langle V_E\rangle'$ increases), as in the formation of ETBs and ITBs. In the latter case, the residual stress and intrinsic rotation profile can exhibit dramatic changes *without* any particular change in confinement, ∇T, ∇n etc! Of course, other scenarios are possible, involving trade-offs between radiative diffusion and wave refraction effects. This issue will be discussed further in section 5.

The issue of symmetry breaking can be profitably illuminated by an approach via radiation hydrodynamics for drift waves, as described here [64, 65]. In this framework, $\langle k_\parallel\rangle = \int {\rm d}\boldsymbol{k} k_\parallel N/\int {\rm d}\boldsymbol{k} N$—i.e. mean $k_\parallel$ emerges from a $k_\parallel$ moment equation of wave kinetics, so the evolution of $\langle k_\parallel\rangle$ is described by a moment equation for $\langle p_\parallel\rangle \sim \int {\rm d}\boldsymbol{k} k_\parallel N$. Wave parallel momentum density calculations give the result:

$$\langle k_\parallel\rangle \simeq \tau^w_{c\boldsymbol{k}}\left\{ -\frac{1}{r}\frac{\partial}{\partial r}[r\langle\Pi^w_{r\parallel}\rangle] - \int {\rm d}\boldsymbol{k}\left(\frac{\partial k_\parallel}{\partial k_r}\right)k_\theta\langle V_E\rangle'\langle N\rangle \right.$$
$$\left. +2\int {\rm d}\boldsymbol{k} k_\parallel \gamma_{\boldsymbol{k}}\langle N\rangle\right\}. \qquad (24)$$

Thus, we see that the net wave momentum density at a given position is determined by the competition between nonlinear decay (i.e. spectral transfer, or scrambling, with correlation time $\tau^w_{c\boldsymbol{k}}$) and the following terms: (a) local inflow or outflow of wave momentum density by transport, given by $-\partial_r\langle\Pi^w_{r,\parallel}\rangle$. (b) enhancement of $\langle k_\parallel\rangle$ via synergy between electric field shear ($\langle V_E\rangle'$) and magnetic shear ($\partial k_\parallel/\partial k_r \neq 0$!). This is the same process as the $\boldsymbol{E}\times\boldsymbol{B}$ shear induced mode shift or eddy tilting process discussed in section 4.1. In eikonal space it may be understood as a process of $k_\parallel$ wind-up due to $\langle V_E\rangle'$ shear-induced *eddy tilting*. Since $\partial k_\parallel/\partial k_r \sim k_\theta$, the overall effect is even in k_θ and $\sim k^2_\theta$. (c) $k_\parallel$ asymmetry in growth rate $\gamma_\parallel$—a rare occurence.

4.3. Boundary asymmetries

This section deals with the effect of boundary asymmetries on intrinsic torque. Here we focus on LSN versus USN asymmetry and its effect on residual stress. This issue is closely related to the well-known LSN and USN asymmetry in the H-mode power threshold.

One of the most persistent puzzles in L $\rightarrow$ H transition phenomenology is why the power threshold is usually lower for LSN configurations (with ∇B drift *into* the X-point) than for USN configurations (with ∇B-drift *away* from the X-point). Here, we briefly summarize recent progress on a model which links this asymmetry to the interplay of magnetic shear and $\boldsymbol{E}\times\boldsymbol{B}$ shear-induced eddy tilting, and its affect on Reynolds stress generated $\boldsymbol{E}\times\boldsymbol{B}$ flows [41]. Simply put, *both* magnetic and electric field shear act to tilt eddys. Tilting eddys induce a perpendicular Reynolds stress, by rendering $\langle\tilde{V}_{r,E}\tilde{V}_{\perp,E}\rangle \neq 0$. Thus, the *local* radial wavenumber is given

by, $k_r(\theta) = k_r(\theta_0) + [(\theta - \theta_0)\hat{s} - V_E'\tau_c]k_\theta$, where the first term is due to magnetic shear tilting (which varies with angle θ) and the second term is due to $\boldsymbol{E} \times \boldsymbol{B}$ shear tilting, which grows in time. Hereafter, we take $\tau = \tau_c$, the turbulent correlation time and thus the eddy life time, and $\theta_0 = 0$. Given the structure of $k_r(\theta)$, the total non-diffusive (i.e. 'residual') Reynolds stress is

$$\langle \tilde{v}_r \tilde{v}_\theta \rangle = \langle \tilde{v}_r{}^2(0) \rangle F^2(\theta)[-\theta\hat{s} + V_E'\tau_c] \tag{25}$$

$F^2(\theta)$ refers to the potential fluctuation intensity as a function of poloidal angle θ.

Now the point here is readily apparent from observing that $\langle \theta F^2(\theta) \rangle_\theta$ will tend to vanish unless there is an imbalance between contributions to the flux surface average from $\theta > 0$ and $\theta < 0$ – i.e. *an up–down asymmetry, as for LSN versus USN*! The remaining question is to determine *when the magnetic shear-induced stress adds to or subtracts from the* $\boldsymbol{E} \times \boldsymbol{B}$ *shear-induced stress and the related flow production.* To do that, the electric field shear must be computed self-consistently, by solving the poloidal momentum balance equation: $\partial_t \langle v_\theta \rangle + \partial_r \langle \tilde{v}_r \tilde{v}_\theta \rangle = -\gamma_{CX} \langle v_\theta \rangle$ where $\langle \tilde{v}_r \tilde{v}_\theta \rangle = -\chi_\theta \partial_r \langle v_\theta \rangle + \Pi_{\hat{s}} + \Pi_{V_E'}$ so

$$\partial_t v_\theta + \partial_r(\Pi_{\hat{s}} + \Pi_{V_E'}) = -(\gamma_{CX} - \partial_r \chi_\theta \partial_r)[V_E + V_{*i}]. \tag{26}$$

Here we have used radial force balance while neglecting toroidal flow, and have accounted for turbulent viscosity (χ_θ) and frictional damping (γ_{CX}), and retained both magnetic shear ($\Pi_{\hat{s}}$) and electric field shear ($\Pi_{V_E'}$) driven residual stresses. Of course, $\langle V_E \rangle'$ in the latter also must satisfy radial force balance. Equation (26) is solved while imposing the boundary conditions $E_r = -3\partial_r T_e$ (i.e. determined by SOL physics) at the LCFS and $V_E = -V_{*i}$ in the core. Assuming gyro-Bohm turbulence and using standard parameters, we calculate V_E/c_s and V_E', as shown in figure 12. It is readily apparent that favourable (i.e. LSN) configurations (where $\Pi_{\hat{s}}$ and $\Pi_{v_E'}$ add) give a larger and stronger edge electric field shear layer than do unfavourable (i.e. USN) configurations (where $\Pi_{\hat{s}}$ and $\Pi_{v_E'}$ subtract). The effect is significant—maximum shears are at least twice as strong for LSN than for USN. The corresponding Reynolds force is obtained, too. We also note that the effect is not poloidally symmetric, when variation of intensity in θ is considered.

The effect on toroidal rotation follows directly from the relation between $\Pi^R_{r\phi}$ and perpendicular Reynolds stress discussed above, i.e. $\Pi^R_{r\phi} \simeq -(B_\theta/B_T)\langle \tilde{v}_r \tilde{v}_\perp \rangle$. The results above immediately suggest that $\partial_r \langle v_\phi \rangle|_a = -(B_\theta/B_T)\langle \tilde{v}_r \tilde{v}_\perp \rangle/\chi_\phi$, so edge rotation gradients differ substantially for LSN and USN. In particular, in the favourable, LSN configuration, $\partial \langle v_\phi \rangle/\partial r|_a > 0$, while for the unfavourable, USN configuration, $\partial \langle v_\phi \rangle/\partial r|_a < 0$. These trends are observed in DIII-D [66] and Tore Supra [67] L-mode. Their implications for central rotation are unclear, as core momentum transport physics also affects central rotation. The relation of these results to the well-known C-Mod experiments of LaBombard *et al* [39] is also unclear, since SOL flow effects appears to be significant in that case. In that vein, some have hypothesized that turbulent viscosity, resulting from parallel shear flow instability [68] of strong SOL flows, may scatter SOL flow momentum through the LCFS and into the core, in such a way as to affect core rotation. In this scenario, poloidally in-out asymmetric particle flux, driven by drift wave turbulence, produces a SOL flow via the symmetry breaking due to magnetic configuration (i.e. LSN versus USN). Transport of this SOL flow momentum into the core plasma is then hypothesized to spin-up core rotation. Of course, the formation of an ETB, as by an L → H transition, will block any influx of SOL momentum into the core, as indeed observed in experiment. This interesting SOL-flow-based scenario, motivated by observed LSN → USN jog induced flow reversals in C-Mod L-mode plasmas, is as yet unsupported by even semi-quantitative theoretical work. The details of how that 'tail wags the dog' mechanism actually works, and how efficient it is, remain exceedingly murky. Note there is a clear distinction between the eddy tilting and SOL flow mechanism. In the eddy tilting scheme, turbulence exerts a stress at the separatrix, the sign of which is partially, but not exclusively, determined by the magnetic geometry. In the SOL flow scheme, turbulence is thought to *transport* momentum from *outside* the separatrix into the core. Differentiating between these two scenarios remains a challenge for experiment.

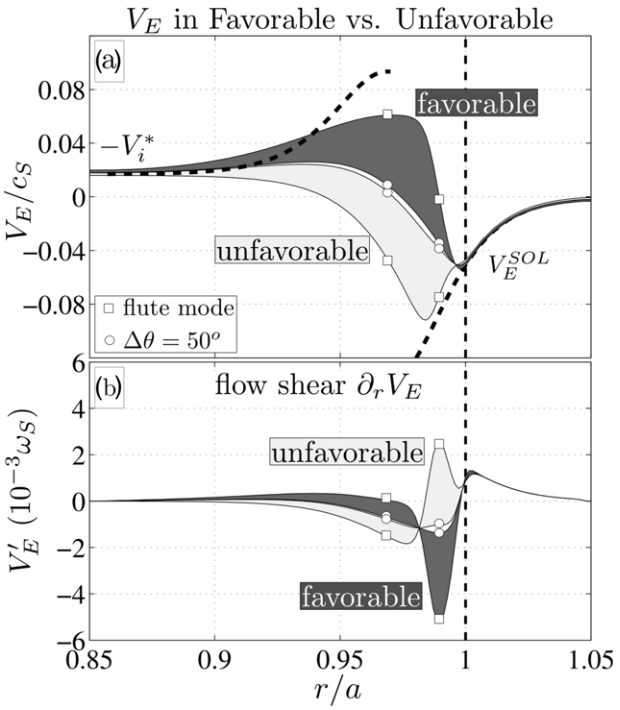

Figure 12. (*a*) Radial profile of $E \times B$ velocity for unfavourable (light grey) and favourable (dark grey) configurations. (*b*) Associated electric shear profile [41].

4.4. Non-local effects and their role in intrinsic torque

Though controversy still persists, there is mounting evidence that turbulent transport in tokamaks is 'non-local', i.e. not well described by a linear, local flux-gradient relation [69]. Specific processes which may be at work include avalanching and turbulence spreading. Thus, non-locality surely must also enter the story of momentum transport and intrinsic torque. However, the evident importance of wave propagation dynamics in the residual stress, along with the rather strong effects of boundary stresses, SOL flows and pedestal intrinsic torque suggest that momentum may, in some sense, be

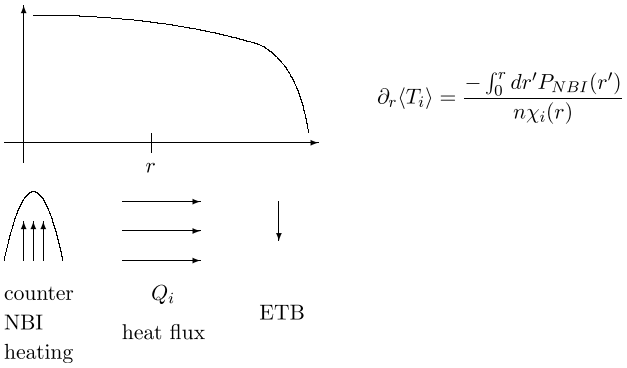

Figure 13. Conventional scenario of finite core $\nabla T_i(r)$ set by heat flux from deposition. ∇T_i steepens at ETB where $\chi_i(r)$ is suppressed.

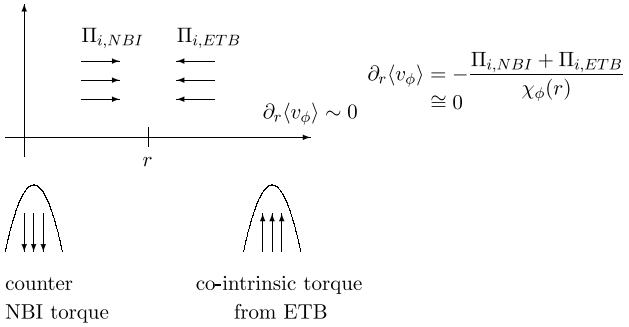

Figure 14. In contrast, core ∇v_ϕ is set by *sum* of *outgoing* NBI torque induced flux and *incoming* intrinsic torque induced flux. These cancel, leaving $\partial_r \langle v_\phi \rangle \cong 0$ in the core. The incoming momentum flux from the ETB intrinsic torque thus gives the *appearance* of a non-locality, in that an edge effect 'back reacts' on the core—a 'tail which wags the dog'. In the Solomon cancellation experiment, the 'tail' and the 'dog' in fact cancel, leaving a flat profile.

'more non-local' than heat transport (figure 13). One striking demonstration of this is the cancellation experiment of Solomon *et al* [21], in which centrally deposited counter-NBI and pedestal co-intrinsic torque combine to yield an essentially *flat* rotation profile, with $\langle v_\phi \rangle = 0$, from $\rho = 0$ to $\rho = 1$. This result suggests a potentially non-local character of momentum transport. In this section, we discuss the theory and simulation of non-locality in momentum transport.

It is interesting and instructive to first observe that the presence of an intrinsic torque can give the naive impression that momentum transport is 'non-local', even within the formulation of a purely local theory! To see this, consider the rather relevant example of the Solomon cancellation experiment—i.e. net counter-NBI torque triggering an L → H transition which produces a co-intrinsic torque in the pedestal. Ignoring the momentum pinch for simplicity, stationary momentum balance for this case gives

$$\partial_r \Pi = T_{\text{ext}}(r) \tag{27}$$

$$\Pi = -\chi_\phi \partial_r \langle v_\phi \rangle + \Pi^{\text{res}} \tag{28}$$

So

$$-\partial_r \chi_\phi \partial_r \langle v_\phi \rangle = T_{\text{ext}}(r) + T_{\text{intr}}(r) \tag{29}$$

where T_{ext} is the external torque (assumed to be peaked on axis) and T_{intr} is the intrinsic torque ($\sim -\partial_r \Pi^{\text{res}}$), and situated in the H-mode pedestal [21]). For simplicity then, we take

$$T_{\text{intr}} = a T_I \delta(r - r_{\text{ped}}) \tag{30}$$

where r_{ped} is the location of the top of the pedestal and T_{I} gives the strength of the intrinsic torque. Here $T_{\text{I}} > 0$ (co-torque) while $T_{\text{ext}} < 0$ (counter-NBI). Then, equation (29) gives

$$\begin{aligned}\partial_r \langle v_\phi \rangle &= -\frac{1}{\chi_\phi}\left[\int_0^r \mathrm{d}r' T_{\text{ext}}(r') + a T_{\text{I}} \Theta(r_{\text{ped}} - r)\right] \\ &= -\frac{1}{\chi_\phi}\left[\int_0^r \mathrm{d}r' T_{\text{ext}}(r') + a T_{\text{I}}\right].\end{aligned} \tag{31}$$

Note that T_{ext} and T_{I} oppose one another. Interestingly, equation (31) suggests that the core velocity gradient $\partial_r \langle v_\phi \rangle$ appears to consist of a usual local piece $\sim \int_0^r \mathrm{d}r' T_{\text{ext}}(r')$, driven by the NBI momentum deposited within the flux surface at r, plus a piece originating from the pedestal *intrinsic* torque, which self-organizes at the edge. The latter has the appearance of a 'non-local', or 'tail-wags-the-dog' effect, since it *originates at the edge yet it dramatically affects the core* velocity profile. Indeed, in the Solomon cancellation experiment, T_{I} cancels T_{ext}, leaving $\partial_r \langle v_\phi \rangle \cong 0$ (figure 14). Thus, we see that localized localized intrinsic torques, such as those due to ETBs and ITBs, can give the appearance of a 'non-local' effect in the momentum balance, in spite of the fact that the basic transport model from which they originate is fundamentally local! This simple example illustrates the subtlety of what may appear as non-locality in momentum transport.

One well-known agent of genuine 'non-locality' is avalanching, as in a sandpile self-organized criticality. Avalanches can produce transient mesoscale and large scale transport events, which connect large regions of the plasma. An avalanche is a burst of correlated transport kicks by interaction between adjacent modes extending over a range of scales $\Delta_c < l < L_{\text{macro}}$. This range falls in the range of mesoscales. Heat flux avalanches have been observed in many simulations [45, 69, 70] and some experiments [71]. An interesting question, then, is how *momentum avalanches* behave in a heat flux-driven state without momentum input (i.e. which corresponds to a state of purely intrinsic rotation). To address this, we report on results of full f, gyrokinetic simulations which compare the probability distribution function of the heat flux and momentum flux [45]. Results are shown in figures 15 and 16. Figure 15 shows that the pdf of the heat flux is very well correlated with the pdf of the negative of the momentum flux, $-\Pi$, i.e. $\text{pdf}(Q) \sim \text{pdf}(-\Pi)$. This suggests that while avalanches transport heat *outwards*, they tend to transport momentum *inwards*. In contrast, figure 16, from the same study but from a different simulation, indicates *outward* avalanching in both heat and momentum. In that case, $\text{pdf}(\Pi) \sim \text{pdf}(Q)$, including the non-Gaussian tail on the pdf. A possible explanation of the origin of the differences between the figures is that the profiles for figure 15 are chosen so that ∇T_{i} is maximal near the *edge*, due to the imposition of an artificial edge cooling. In some sense, the simulation resembled an RI-mode plasma [72, 73], the edge of which is strongly cooled by radiation due to impurity injection. Thus, the heat engine picture (which links

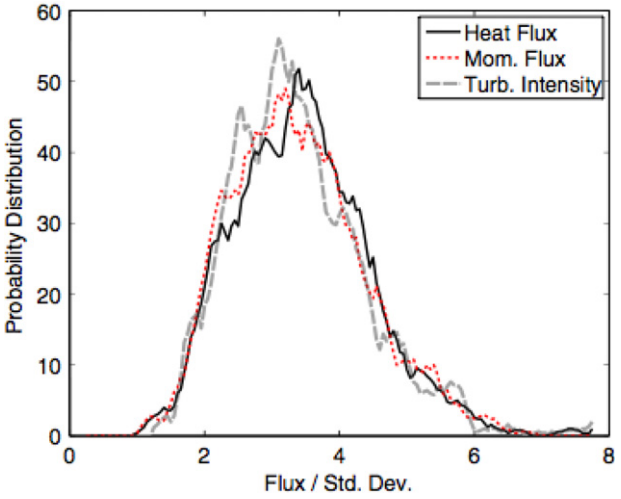

Figure 15. Pdf for heat flux and momentum flux with ∇T_i maximal at the edge. Here, Pdf(Q)∼Pdf($-\Pi$), indicating close correlation by opposite sign of the fluxes.

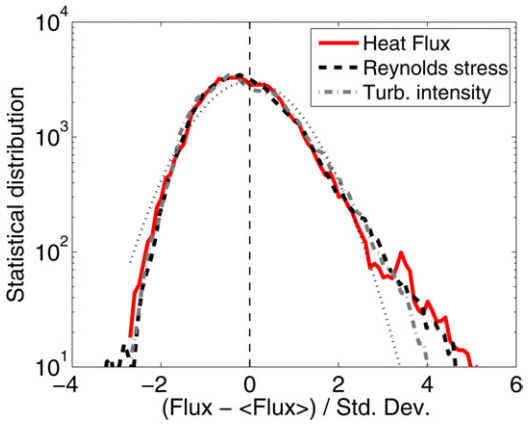

Figure 16. Pdf for heat flux and momentum flux with ∇T_i freely evolving, becoming maximal at the core. Here, Pdf(Q)∼Pdf(Π), indicating close correlation and like direction of the fluxes.

Π^{res} to ∇T_i) tells us that it is not surprising that intrinsic rotation is driven from the edge inwards. In case of figure 16, ∇T_i evolves so there are turbulence and avalanches throughout the domain, and ∇T_i is largest in the core. In that case, an in → out development is to be expected, and is indeed realized. The contrast between these two cases nicely illustrates the impact of the *global* configuration, boundary conditions, etc. on the development of the *local* structure of intrinsic rotation. Such sensitivity to global structure can appear as 'non-locality'.

We briefly comment here on what might qualify as an unambiguous signature of non-locality in intrinsic torque. Gyrokinetic simulations [70] have noted the existence of a non-local relation between the turbulent heat flux Q_i and ∇T_i, given by $Q(x) = -\int dx' \kappa(x, x') \nabla T_i(x')$. Here, $\kappa(x, x')$ is a non-local kernel $\kappa \cong S_0/\{(x - x')^2 + \Delta^2\}$, and $L_{T_i} > \Delta > \Delta_c$. Note that $\int dx' x'^2 \kappa(x - x')$ diverges, suggesting that the avalanches produce Levy flights as the origin of non-locality. For $\nabla v_\phi \neq 0$, one would straightforwardly expect that the diagonal part of the momentum flux would exhibit a similar relation between Π_{diag} and ∇v_ϕ, as a generalization of $\chi_\phi \sim \chi_i$. More interesting, however, is the possibility that $\Pi^{res}(x) \sim \int dx' \alpha(x, x') \nabla T_i(x')$, suggesting a non-local relation between residual stress and ∇T_i! Here, $\alpha(x, x')$ is an interaction kernel, related, but not necessarily identical to, $\kappa(x, x')$. Such a relation is the logical non-local extension of the $\Pi^{res} \sim \nabla T_i$ proportionality discussed at length above, in the context of the engine model. We remark that it would be quite interesting to investigate simulation data for evidence of such a dependency.

Turbulence spreading-induced non-locality can also occur from radiation transport of wave momentum by drift waves. This idea builds upon the relation between wave propagation and momentum transport, discussed above. A straightforward calculation, which extends the Chapman–Enskog analysis discussed in [31], yields the mean flux of parallel wave momentum:

$$\langle \Pi^w_{r\parallel} \rangle = -D_w \frac{\partial}{\partial r} \langle p^w_\parallel \rangle + V_w \langle p^w_\parallel \rangle, \tag{32}$$

where $D_w = \int d\boldsymbol{k} (v_{gr}(\boldsymbol{k})^2/\nu_k) \langle N \rangle / \int d\boldsymbol{k} \langle N \rangle$ is the drift wave quanta diffusion coefficient and $V_w = -\int d\boldsymbol{k} [\partial/\partial k_r (v_{gr}(\boldsymbol{k})/\nu_k) k_\theta \langle v_E \rangle' \langle N \rangle / \int d\boldsymbol{k} \langle N \rangle]$ is the quanta convection velocity, which is driven by $\langle v_E \rangle'$, and $\nu_k = (\tau^w_{c,\boldsymbol{k}})^{-1}$ is the wave packet decorrelation rate. For turbulence levels near the mixing length level, $D_w \sim D_{GB} = \rho_s^2 c_s / a$. Thus, we see that non-resonant ion momentum is transported by diffusive wave scattering and shearing-induced convection. Of course, conservation of total momentum requires an adjustment in mean flow momentum in response to that of the wave momentum, thus leading to observable flow profile evolution. This shows that the close connection between non-resonant particle momentum and wave momentum allows us to write an explicit, if somewhat theoretical, expression for the diffusive and convective mean wave momentum flux, which is given in equation (32). This supports the heuristic arguments for the role of turbulence spreading in intrinsic rotation dynamics, and strengthens the case that calculations of intrinsic torque must address non-locality. In particular, this simple example tells us (a) to expect a non-trivial 'convective' contribution to the residual stress due to wave transport, and (b) that a more fundamentally sound approach to modelling intrinsic rotation and momentum transport must evolve the wave kinetic distribution (with spreading effects!) along with the profiles.

5. Theory meets the phenomenology: a critical appraisal

In this section, we discuss how the theory of intrinsic torque fares upon confrontation with the phenomenology. The aim here is to assess what is understood, where understanding is developing, and what remains poorly understood. We do not pretend to present a complete discussion, but rather a survey of key points. A full review of the many interesting results on intrinsic rotation, and our theoretical understanding thereof, is far beyond the scope of this OV paper. Here we focus on issues which are critical to the theory discussed here. This discussion is organized into sections on: (a) general aspects of intrinsic torque, (b) intrinsic rotation in ETB, (c) intrinsic torque in ITB, (d) OH reversals, (e) intrinsic torque effects in co-NBI H-mode with ECH, (f) LSN ↔ USN asymmetry

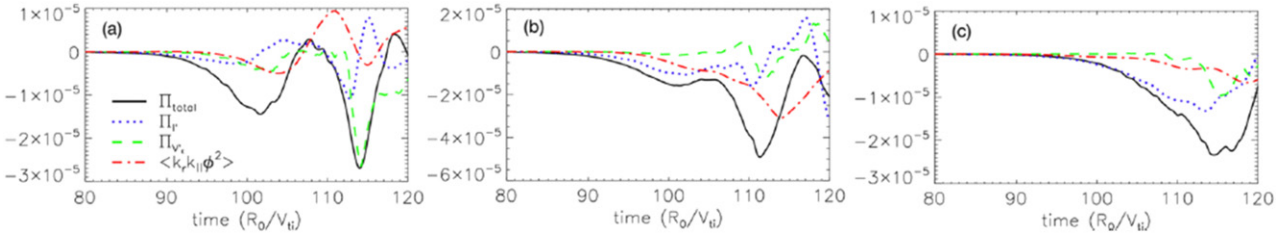

Figure 17. Audit of residual stress contributions from gKPSP simulations [55]. Both $E \times B$ shear and intensity gradient contributions are substantial and comparable. This figure shows there is no clearly and universally dominant symmetry-breaking mechanism which controls the residual stress.

and L-mode flow reversals. The important topic of intrinsic rotation in LHCD is beyond the scope of this paper and left for future reviews.

5.1. General aspects

From sections 3 and 4, we saw that the essential elements of the theory are the engine paradigm and the basic aspects of symmetry-breaking mechanisms. Regarding the engine paradigm, figure 5 illustrates the linear proportionality of intrinsic torque (as measured from GK simulation of ITG turbulence) to R/L_T [45, 74]. Similar results have been obtained from simulations of CTEM [46], i.e. $\tau \sim 1/L_{T_e}, 1/L_n$, as shown in figure 6. Several physical experiments support the heat engine concept that V_ϕ tracks ∇T [8, 10, 44]. The dynamic response has not yet been addressed, i.e. the question of 'is there a time delay between the responses of ∇T and perturbation experiments?' remains unanswered. Interestingly, there is some hint from simulations that such a time delay is, in fact, present [45]. Regarding symmetry breaking, figure 17 shows the decomposition of residual stress obtained from GK simulation [55] into pieces proportional to $\langle V_E \rangle'$, I', etc. Not surprisingly, under standard conditions there is no clearly dominant piece, and *all* seem to contribute. Most dedicated simulation studies confirm the basic ideas on symmetry breaking and its role in residual stress, which were discussed in section 4. Apart from indirect inference from profiles, physical experiments have not been able to address the theory of symmetry breaking, since to do so requires careful measurement of the off-diagonal components of the Reynolds stress tensor. It is also worth noting that simulations have recovered the build-up of *net macroscopic* intrinsic rotation, as shown in figure 18 from [45]. Likewise, numerical cancellation experiments, after Solomon, have been performed successfully.

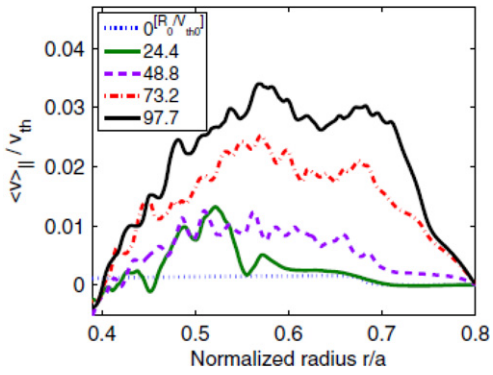

Figure 18. Profile evolution in GYSELA simulation [45]. Note that a flow with net momentum builds up from noise during the simulations.

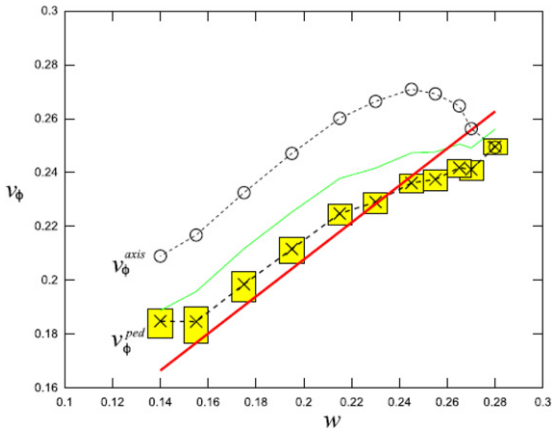

Figure 19. The relation between toroidal velocity and pedestal width obtained from the solution of a reduced model [75]. The figure shows that the velocity at the top of the pedestal increases with the width of the pedestal.

5.2. H-mode ETB and pedestal intrinsic torque

The most studied case of intrinsic torque is that located in the H-mode pedestal. This is then a natural phenomenon to attack by modelling. Prime goals are to recover the Rice scaling trend, and understand their underpinning. A reduced model based on transport bifurcations in the presence of $\langle V_E \rangle'$-triggered intrinsic torque was developed [75]. Figure 19 illustrates aspects of the edge rotation profile obtained from this simple model by showing the (approximately) linear proportionality of velocity at the pedestal to the pedestal width. Qualitatively good results are obtained—i.e. the intrinsic rotation pedestal builds up as part of the process of ETB formation. The rotation pedestal clearly builds from the boundary inwards. Results also indicate that the pedestal width effectively determines the height of the rotation pedestal, i.e. $\Delta V_\phi \sim (w/a) V_{Thi}$, and $\Delta W \sim w$ (increment in stored energy scales with pedestal width). Thus, the dynamics are consistent with the Rice scaling. If we use a frequently invoked semi-empirical expression for the pedestal width w, i.e. $w \sim \sqrt{\beta_p} a$ [76], the Rice scaling follows directly. Attempts to recover the I_p^{-1} trend of the Rice scaling from simulation studies of q or $\hat{s}$ dependence have also been successful, but are not entirely in agreement with one another [46, 55]. All results suggest that

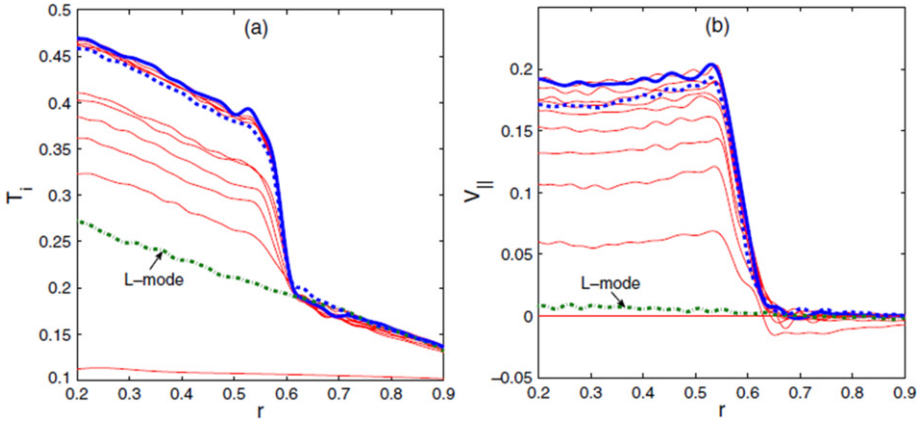

Figure 20. Reversed shear ITB profiles from TRB GF simulations of ITG turbulence with Boltzmann electrons and no-slip boundary conditions [79]. The ITB foot is located at $r = 0.6$. Strong intrinsic rotation builds within the ITB. Clearly, $\Delta\nabla v_\phi \sim \Delta\nabla T_i$, i.e. ∇v_ϕ steepens with increasing ∇T_i.

the Rice scaling is a macroscopic realization of the engine paradigm and the fundamental $\nabla V_\phi \sim \nabla T$ scaling trend. We also comment that the central velocity evolution (in terms of which the Rice scaling is stated) may be affected by additional physics, such as a momentum pinch. Finally, we note that the proposed mechanism of orbit loss—which seems to survive countless silver stakes driven through its heart—has also been suggested as a driver of ETB-related intrinsic rotation [78]. For orbit loss, $\Delta v_\phi \sim \Delta T$, rather than $\Delta\nabla v_\phi \sim \Delta\nabla T$, is predicted to be the key macroscopic scaling correlation. We remark here that a careful study of the available edge rotation data should be undertaken to compare these two predictions. Published results from Alcator C-Mod are *not* consistent with the orbit loss paradigm [8]. Finally, there is a clear need for relevant fluctuation studies—including direct Reynolds stress measurements—in regions beyond the base of the pedestal.

5.3. Intrinsic rotation in ITBs

Rather little is known about intrinsic rotation in ITBs and the role of intrinsic torque in ITB dynamics, apart from experiments from C-Mod [22–25] and Large Helical Device (LHD) [10]. Here, we discuss a few aspect of the results from recent TRB simulations of reversed shear ITB dynamics [79]. These simulations are flux-driven gyrofluid (GF) studies of ITG turbulence [80–83] which omit the effect of non-resonant modes. These simulations may not be directly relevant to the ITBs in Alcator C-Mod, where ∇n steepening occurs and turbulence is likely collisionless trapped electron mode (CTEM) [25]. Modulo the difference in magnetic configurations of a tokamak and stellarator, they are, however, relevant to LHD.

Simulation results indicate that ITBs form, and intrinsic rotation develops, inside of the barrier location. This is shown in figure 20. The Reynolds stress can be shown to be decomposed into an outward diagonal diffusive piece plus an inward residual, as shown in figure 21. The central velocity scales with ∇T_i, until ITB suppression of turbulence to levels where $\chi_i^{\text{Turb}} \leqslant \chi_i^{\text{neo}}$ is achieved, as shown in figure 22. At that point, neoclassical Prandtl number dependence (i.e. dependence upon the ratio of neoclassical χ_ϕ and neoclassical χ_i—namely $\chi_\phi^{\text{neo}}/\chi_i^{\text{neo}}$) appears in $\langle V_\parallel(0)\rangle$ scaling trends, on account of the difference between the residual transport of momentum and heat. This Prandtl number dependence is also related to the strength of relative hysteresis between ∇V_ϕ and ∇T_i, which is observed in experiments. The strength of the relative hysteresis of ∇V_ϕ with ∇T_i decreases with neoclassical Prandtl number, as shown in figure 23, and seen in experiment [10]. All told, results from experiment and this rather basic simulation track expectations based on simple ideas about ITBs, and on our experience (in both theory and experiment) with ETBs. Considerable further study of ITBs controlled by CTEMs is required. There, interaction of particle and momentum transport will be especially important. Interaction and possible competition between core and edge intrinsic torque are particularly important issues. We remark that intrinsic torque in ITBs rather clearly merits more study, both as a means to test the theory and models, and as a central element in a scenario for 'de-stiffened low torque core confinement' [77].

Since this section has stressed the similarity between ETB and ITB intrinsic torque, we remark on a few possible differences. One major distinction is the possible role of manifestly boundary-related effects in the ETB core. These include upper and lower null point (USN versus LSN) asymmetry, SOL flows, and orbit loss. Another possible distinction is the ITG versus CTEM competition, which is more likely in the core. Thus, care must be taken to avoid over generalization from ETB to ITB.

5.4. OH reversals

The interesting subject of OH reversals was discussed in some detail in section 2. Two central questions must be addressed by experiment in order for a meaningful confrontation with theory to occur. To test the key idea that the OH inversion is a consequence of a change in the sign of Π^{res} due to a mode population change or 'flip' from TEM ($\sim v_{*e}$) to ITG ($\sim v_{*i}$) as confinement saturates, experiments must:

(i) find some indication, likely from macroscopics, of the mechanism of symmetry breaking in this regime. It is far from clear that the conventionally invoked $\langle V_E\rangle'$, or more generally, 'profile shearing' [32] is the dominant

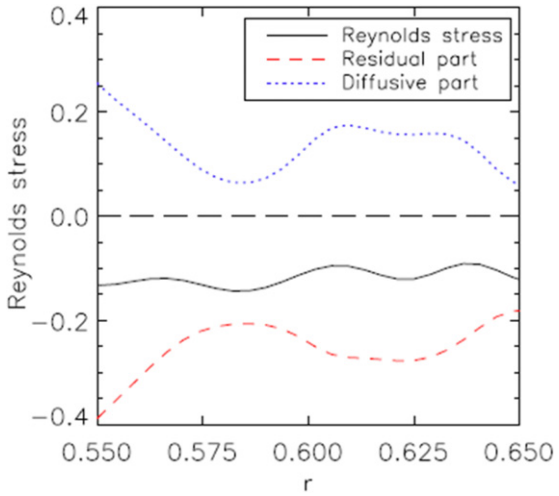

Figure 21. Decomposition of Reynolds stress in the same ITB simulations as figure 20 [79]. An inward, non-diffusive residual stress is evident.

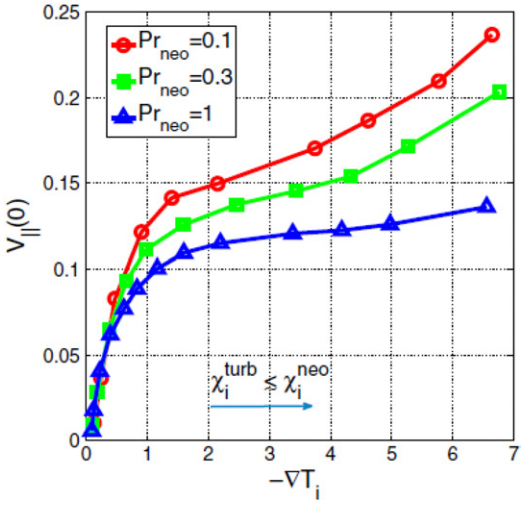

Figure 22. $\langle v_\parallel(0)\rangle$ versus $-\nabla T_i$ for ITB intrinsic rotation plotted for different neoclassical Prandtl numbers [79]. Note that a linear phase at lower $-\nabla T_i$ (akin to Rice scaling), is followed by saturation when the ITB quenches turbulence, and a subsequent slight increase due to relative hysteresis.

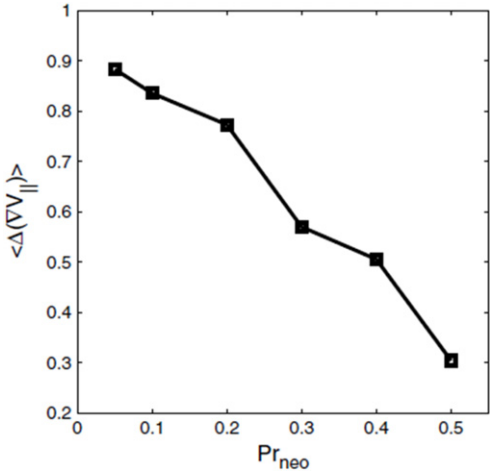

Figure 23. Change in $\nabla V_\parallel$, plotted versus neoclassical Prandtl number [79]. The scaling is suggestive of relative hysteresis.

mechanism in this regime. Intensity gradient and the wave stress are viable alternative mechanisms,

(ii) perform coordinated fluctuation measurements which unambiguously show a temporally coincident reversal in the sign of the centroid of the frequency spectrum *in the region* which controls the inversion. Note that this amounts to revisiting earlier measurements [84] on fluctuation spectral changes as n crosses n_{sat}, in concert with rotation profile studies.

Neither of these central questions has been substantively addressed by experiment. Though some hints of changes in fluctuation spectra have been observed during C-Mod reversals, the evidence for a mode shift is far from conclusive [27–29]. Theory has addressed the second question but has largely ignored the first, while sticking to the conventional wisdom concerning symmetry breaking. Furthermore, theory has not substantively addressed the important and interesting phenomenon of density hysteresis [26, 27], the role of boundary conditions (results from TCV [26, 30] indicate a change in direction between limited and diverted OH plasmas, other factors being equal) or the origin and meaning of boundary rotation spikes [28]. An interesting suggestion concerning the impact of non-locality effects has recently appeared [69, 85], but needs further development.

A speculative digression on the physics of OH reversals seems appropriate here. First, the OH-reversal is a rather clear-cut example of the second class of momentum transport bifurcation discussed in section 4.3, in which $\Pi^R_{r,\parallel}$ flips sign but confinement does not change. This idea and observation go hand-in-hand with the hypothesized 'mode flip' scenario. However, the observed hysteresis in density tells us clearly that *some asymmetry between transient states of increasing and decreasing density is present.* A hypothesis for the origin of such asymmetry is that it is a consequence of the inter-penetration of two competing gases of drift or ITG mode quasiparticles, representative of TEM and ITG turbulence respectively. In this picture, the plasma consists of TEM regions, ITG regions, and 'mixed states', where both populations coexists. Thus, as n increases, one might expect the ITG population to advance or 'spread' into the TEM population and eventually squeeze it out. For decreasing n, one might expect the reverse, but with a different front speed—hence the hysteresis. This idea presents a real challenge to both simulation and experiment—i.e. for the former to realize a macroscopic inversion and for the latter to achieve what amounts to 'fluctuation propagation direction imaging'. In this regard, nonlinear global delta-f gyrokinetic particle simulations with the gkPSP code [86] have indeed noted 'inverted' rotation profiles when comparing otherwise similar ITG and TEM dominated states [86]. This is shown in figure 24. These results are the first non-trivial hint from *nonlinear* gyrokinetic simulation that the 'mode flip' scenario is viable. Much further work is required, however. It does seem fair to say, though, that a purely quasi-linear approach which ignores mixed states is *too simple*. At this stage, the bottom line is that while the theory and experiment of OH reversals have independently accomplished a significant amount, they are only beginning to connect.

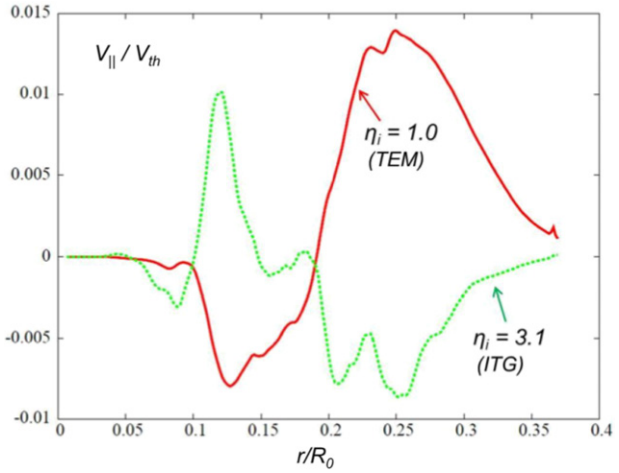

Figure 24. gkPSP simulation of toroidal flow profile before and after change from TEM → ITG state [86]. Note that the profiles are suggestive of an inversion.

5.5. ECH + co-NBI H-mode and ECH H-mode

Understanding rotation in H-mode discharges with combined co-NBI and ECH, and in H-mode discharges heated by ECH only, is a high priority issue for ITER. Thus, it is puzzling as to why a greater effort to understand the structure of the resulting rotation profiles has not been made. Several experiments [34–36, 87] tell us that for co-NBI with modest levels of ECH, the effective torque balance is central co-NBI torque plus pedestal co-intrinsic torque versus central counter-torque associated with ECH. However, we note that this trend is not universal since counter intrinsic rotation with ECH + co-NBI H-mode was observed in JT-60U [33]. Exceptions do exist, however. For pure ECH cases, the trend is a core counter torque and rotation (consistent with the ECH+NBI findings) [35, 87], and a pedestal co-torque and co-rotation. A connection region or transition layer, where v_ϕ passes through zero, links the counter rotating core and the co-rotating edge pedestal regions. The implications of what would happen if the $v_\phi = 0$ point were located near the $q = 2$ radius of ITER are unpleasant to contemplate. At the microscopic level, the central question is the physics origin of the ECH-related intrinsic counter torque. At the macroscopic level, an interesting question is why a connection layer appears between a counter-core and co-pedestal, in contrast to the cancellation experiments, where core counter-NBI plus co-pedestal intrinsic torques combine to produce a *flat* rotation profile. Related to this, the extent of the central region with $\Delta v_\phi < 0$ (i.e. the location of the so-called pivot radius—analogous to the pivot point in inversions) and the magnitude of Δv_ϕ are relevant issues for the co-NBI+ECH cases.

Regarding the issue of the microscopic foundations of the putative ECH-induced counter intrinsic torque, the observed correlations of $1/L_{v_\phi}$ with $1/L_{T_e}$ and/or $1/L_n$ [38] and the steepening of ∇T_e and ∇n in the core have motivated the hypothesis that the ECH induces a flip in core turbulence from ITG to TEM, with a resulting change in intrinsic torque from co to counter [34, 36, 38]. Note that ITG modes (v_{*i} direction) tend to drive co-direction torque (with intensity gradient symmetry breaking), while trapped electron modes

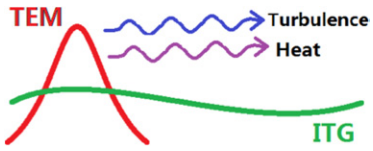

Figure 25. A cartoon of the spatial spreading of TEM turbulence into ITG turbulence. The direction of TEM turbulence spreading is the same as that of the heat flux from the core to the edge.

(v_{*e} direction) tend to drive counter-direction torque [88]. Also note that the structure and evolution of the density profile are critical here, since peaked ∇n profiles favour TEM. Collisionality is also very important [28]. In NBI + ECH, some on-axis peaking of ∇n is observed, which will hasten the flip from ITG to TEM. Clearly, momentum and particle transport are strongly coupled in this instance [87]. We add the cautionary comment that more work on the global dynamics of the reversal mechanism would be helpful to understand that phenomenon. In pure ECH drive, $n(r)$ is relatively flat, so the path to the development of TEM is not so clear. Of course, at higher density, collisional coupling of the species may heat the ions and thus maintain the primacy of ITG. Reconciling the fact that core intrinsic torque is clearly counter in both ECH+co-NBI and pure ECH with the fact that ∇n peaks in the NBI cases but is flat for the pure ECH cases is a challenge for theory. Amazingly, though, despite the wealth of macroscopic profile data and trends, *very little* in the way of simple *linear microstability analysis using experimental profiles* has been undertaken, and *no relevant fluctuation measurements are available*. A recent study of KSTAR profiles from ECH+NBI discharges [36] indicates that a mode population change *may* occur, but is *rather* localized to the deep core. Results are extremely sensitive to ∇n evolution. Further study is required, and consideration should be given to heat avalanching, and turbulence propagation, both of which might 'spread' the domain of TEM excitation, once it is established. A cartoon of this process is shown in figure 25. Of course, mixed states, as sketched in figure 26, are likely to be encountered. Another issue—virtually unmentioned except in very recent work [36]—is the mechanism of symmetry breaking in the core of ECH + NBI plasmas. Results indicate that $V_{E\times B}$ actually *decreases* when ECH is applied, in contrast to what happens in transport barriers. The strong steepening of ∇T_e suggests that the TEM intensity gradient is a prime candidate mechanism. For $I'/I \sim 1/L_{T_e} > 0$, results predict co-torque for ITG and counter-torque to TEM, with the strength of the TEM-induced counter torque $\tau_{TEM} \sim 1/L_{T_e}$. Note that $1/L_{T_e}$ is actually an *underestimate* of I'/I for TEM. Further work on this issue is needed and ongoing. Clearly the full picture for the I' scenario must involve consideration of turbulence spreading, as depicted in figures 25 and 26.

5.6. LSN ↔ USN *asymmetry*

This is an important topic, which has received rather little attention, from either theory or experiment. Apart from the pioneering work of LaBombard *et al* [39], experimental studies have focused on edge profile measurements, but have not addressed dynamics. Theoretical work has confronted the question of magnetic shear + electric shear-induced boundary

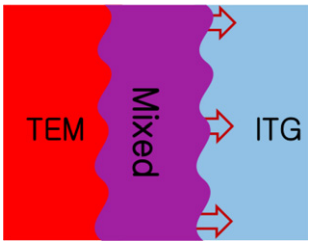

Figure 26. A cartoon of the advance of TEM turbulence into ITG turbulence mediated by a mixed state buffer zone where the two modes co-exist. Here the advance is left-to-right, which corresponds to core-to-edge. The region of the mixed state corresponds loosely to the neighbourhood of the pivot point.

stresses [41], but has not confronted the alternative scenario of how SOL flows might penetrate the core or influence core rotation. It is interesting, though, that results from DIII-D and Tore Supra agree with the model of Fedorczak *et al* [41], as mentioned in section 4. This hints that the scenario of LaBombard *et al* [39] may not be universal, or that it is coupled to eddy tilting processes [41]. Considerations concerning SOL flow effects are limited to discussions of the parallel shear flow instability. In particular, the interaction of shear SOL flows with boundary stresses seems likely to introduce a new element in the eddy tilt-induced shear stress discussed in [41]. This will surely impact the edge stresses which control intrinsic toroidal flows. Of course, perpendicular stresses can drive intrinsic *toroidal* rotation, via the mechanism discussed in section 4.4. Clearly, there is much room for future work in theory, experiment, and simulation.

6. Discussion and conclusion

6.1. Assessment

In this section, we present the conclusions of this OV of intrinsic torque. The conclusions are presented and discussed in the form of an assessment—i.e. outcomes are grouped according to: (i) What we understand well, (ii) What we *think* we understand, but could benefit from improvement in our comprehension, (iii) What we *don't* understand.

(i) What we understand well.

(i) Residual stress and intrinsic torque are driven by parallel and (via projections) perpendicular Reynolds stresses. Momentum convection *together with* a finite flow at the boundary can also drive intrinsic rotation.

(ii) The heat engine paradigm of intrinsic rotation provides a unifying framework within which to develop the theory in terms of fluctuation entropy evolution.

(iii) The residual stress is driven by the thermodynamic forces ∇T, ∇p, ∇n, and produces a local intrinsic torque $-\partial_r \Pi^{\mathrm{R}}_{r,\phi}$. Residual stress can spin up the plasma from rest, acting in concert with boundary conditions.

(iv) Residual parallel Reynolds stress requires symmetry breaking, so as to convert radial inhomogeneity into parallel spectral asymmetry. Symmetry-breaking mechanisms include electric field shear $\langle v_E \rangle'$ and intensity gradient I'—both of which are self-reinforcing and linked to the driving heat flux. Additional symmetry-breaking sets the polarization stress ($\langle k_r k_\parallel \rangle \neq 0 \rightarrow$ essentially a quadrupole spatial moment of the spectrum is required) and the poloidal Reynolds stress, which drives flow through $\langle J_r \rangle B_\theta / c$ (again, $\langle v_E \rangle'$ and intensity gradient are the key elements).

(v) For ITG turbulence, Π_{res} increases with $R/L_{\mathrm{T}} - R/L_{\mathrm{T}c}$, or more generally ∇T_{i}.

(vi) Residual stress is also robust in TEM. TEM-driven residual stress scales with ∇T_{e} and ∇n. The direction of intrinsic torque produced by TEM turbulence can differ from that produced by ITG turbulence.

(vii) Net intrinsic rotation (i.e. an increase in radially *integrated* momentum) with a peak thermal Mach number $M_{\mathrm{T}} \equiv \langle v_\parallel \rangle / v_{\mathrm{thi}}$ of $0.05 < M_{\mathrm{T}} < 0.15$ can be produced in flux-driven ITG simulations with no-slip boundary conditions. Multiple symmetry-breaking mechanisms can, and do, operate simultaneously. Avalanches in heat and momentum are observed, and introduce non-locality to momentum transport.

(viii) Strong intrinsic rotation can be generated by flux-driven ITG turbulence in reverse shear ITBs with off-axis minimum $q(r)$, with no-slip boundary conditions.

(ii) What we think we understand but would benefit from more work on.

(i) The importance of the mechanisms for generation of toroidal rotation by fluctuation-driven radial currents—i.e. via the toroidal projection of the perpendicular Reynolds stress—needs to be assessed more accurately. Similarly, the polarization stress merits deeper thought.

(ii) The basic structure of the Rice scaling ($\Delta v_\phi \sim \Delta W_{\mathrm{p}} / I_{\mathrm{p}}$) originates from (a) strong localized temperature gradients, as in the pedestal and ITBs (i.e. the local origin of ΔW_{p}) and (b) $q(r)$ scaling (i.e. the origin of I_{p}). It is not yet entirely clear how we relate the problem of pedestal intrinsic torque to that of the scalings of the H-mode pedestal width.

(iii) Relative hysteresis of ∇v_ϕ and ∇T_{i} in ITG intrinsic rotation, and its relation to neoclassical Prandtl number Pr_{neo}. These have been observed in experiments [10] and in simulations [79] of ITG turbulence with ITBs. Relative hysteresis is likely present in the H-mode pedestal.

(iv) The precise relation between turbulence propagation direction (i.e. $v_{*\mathrm{e}}$ versus $v_{*\mathrm{i}}$) and toroidal rotation direction has not yet been established. More generally, our understanding of OH reversals and other momentum transport bifurcations not related to confinement bifurcations is still developing.

(v) Non-locality in momentum transport and intrinsic torque is not understood. Seminal ideas have been proposed but not critically analysed. Fundamental theoretical work at the level of phase space entropy dynamics is required.

(vi) How pinch and intrinsic torque might interact to form global profile structure needs further study.

(vii) The question of how intrinsic rotation in H-mode and in ITBs ultimately saturates needs further consideration.

(iii) What we do not yet really understand.

(i) The interplay of turbulence and wave scattering with possible neoclassical effects and orbit loss in determining the boundary condition for intrinsic torque is not understood, at all.

(ii) Our understanding of the detailed interplay between core and pedestal intrinsic torques and the edge boundary physics, and their roles in determining global profiles is in its infancy. This is a *critical issue*.

(iii) The connections between edge eddy tilting, edge stresses, SOL flows and core rotation are unclear. Several scenarios have been proposed, but not analysed.

(iv) The apparent absence of ρ_* scaling of intrinsic rotation signals a major gap in our understanding.

(v) The effect of energetic particles on intrinsic rotation and torque are unknown.

(vi) Models for the detailed spatio-temporal dynamics of intrinsic rotation profile build-up, degree of non-locality, etc are not available.

(vii) The critical torque-to-power ratio that likely delimits pinch versus residual stress dominated momentum transport regimes is unknown.

(viii) The physics of H-mode rotation profiles with competing and interacting NBI torque and ECH driven intrinsic torque is unclear. Pure ECH H-mode rotation profiles are also not understood. Two particular enigmas of the latter are the apparent sensitivity to deposition location and the structure and location of the core-pedestal connection layer. Resolution of these questions requires an understanding of mixed states and the role of turbulence spreading.

(ix) Intrinsic torque and rotation in LHCD and ICRF driven discharges are poorly understood. Of particular note is the apparent change in the sign of the residual stress as LH power is increased [89].

6.2. Programmatic suggestions

Since the principal purpose of the IAEA FEC is to identify topics of programmatic focus, the paper concludes with a section of highly simplified programmatic suggestions. These are as follows.

(i) Contrary to the conventional wisdom, the problem of intrinsic rotation is *not* 'solved'. Research must continue. Certain aspects of the ECH-driven rotation problem seem especially critical (and dangerous) for ITER. The $v_\phi(r) = 0$ null point which appears in ECH H-mode with counter-core and co-pedestal profiles is potentially deadly and merits *much* more attention.

(ii) Fluctuation studies *must* be undertaken in concert with macroscopic profile experiments. Direct measurements of Reynolds stress by HIBP and other means should be pursued.

(iii) OH reversals and co-NBI H-mode + ECH have many elements in common and should be pursued as part of a comparative study, including studies of fluctuation populations, particle transport, and momentum transport.

(iv) Comparative studies of related phenomena with different boundary conditions (i.e. limited L-mode, diverted L-mode, H-mode) would be extremely interesting and useful. OH reversals and the ECH-related phenomena are particularly strong candidates for this sort of study.

(v) Modelling and theory studies must address the question of global profile structure, not only local stresses and gradients. In particular, the incidence of global structural bifurcations should be investigated.

(vi) Much greater attention should be given to *dynamic* (i.e. perturbative) studies of intrinsic torque, and to investigations of related non-locality phenomena.

(vii) The effect of boundary stresses and SOL flows on core rotation is poorly understood and requires much more work.

Clearly, the physics of intrinsic torque still offers many fascinating challenges.

Acknowledgments

The authors thank M. Yoshida, G. Tynan, X. Garbet, V. Naulin, K. Itoh, S.-I. Itoh, A. Bortolon, A.P. Sun, K. Burrell, Z. Yan and M. Xu for stimulating discussions. We also thank members of the CMTFO (Center for Momentum Transport and Flow Organization) at UCSD and participants in the 2009 and 2011 Festival de Theorie (CEA, France) for useful discussions and encouragement. We acknowledge the WCI Program of KNRF and the US DOE for financial support of this work.

References

[1] Ida K. *et al* 1995 *Phys. Rev. Lett.* **74** 1990
[2] Rice J.E. *et al* 1999 *Nucl. Fusion* **39** 1175
[3] Rice J.E. *et al* 2004 *Nucl. Fusion* **44** 379
[4] Rice J.E. *et al* 2007 *Nucl. Fusion* **47** 1618
[5] Whyte D.G. *et al* 2010 *Nucl. Fusion* **50** 105005
[6] Hubbard A.E. *et al* 2011 *Phys. Plasmas* **18** 056115
[7] Kosuga Y. *et al* 2010 *Phys. Plasmas* **17** 102313
[8] Rice J.E. *et al* 2011 *Phys. Rev. Lett.* **106** 215001
[9] Yan Z. *et al* 2010 *Phys. Rev. Lett.* **104** 065002
[10] Ida K. *et al* 2010 *Nucl. Fusion* **50** 064007
[11] Peeters A.G. *et al* 2011 *Nucl. Fusion* **51** 094027
[12] Angioni C. *et al* 2012 *Nucl. Fusion* **52** 114003
[13] Mattor N. *et al* 1988 *Phys. Fluids* **31** 1180
[14] Scott S.D. *et al* 1990 *Phys. Rev. Lett.* **64** 531
[15] Yoshida M. *et al* 2006 *Plasma Phys. Control. Fusion* **48** 1673
[16] Yoshida M. *et al* 2008 *Phys. Rev. Lett.* **100** 105002
[17] Diamond P.H. *et al* 2009 *Nucl. Fusion* **49** 045002
[18] Itoh K., Itoh S.-I. and Fukuyama A. 1999 *Transport and Structural Formation in Plasmas* (Bristol: Institute of Physics Publishing)
[19] Labit B. *et al* 2011 *Phys. Plasmas* **18** 032308
[20] Yoon E.S. and Hahm T.S. 2010 *Nucl. Fusion* **50** 064006
[21] Solomon W.M. *et al* 2007 *Plasma Phys. Control. Fusion* **49** B313
[22] Rice J.E. *et al* 2001 *Nucl. Fusion* **41** 277
[23] Rice J.E. *et al* 2002 *Nucl. Fusion* **42** 510
[24] Rice J.E. *et al* 2003 *Nucl. Fusion* **43** 781
[25] Fiore C.L. *et al* 2012 *Phys. Plasmas* **19** 056113
[26] Bortolon A. *et al* 2006 *Phys. Rev. Lett.* **97** 235003
[27] Rice J.E. *et al* 2011 *Phys. Rev. Lett.* **107** 265001
[28] Rice J.E. *et al* 2011 *Nucl. Fusion* **51** 083005
[29] Rice J.E. *et al* 2012 *Phys. Plasmas* **19** 056106
[30] Duval B.P. *et al* 2008 *Phys. Plasmas* **15** 056113
[31] Diamond P.H. *et al* 2008 *Phys. Plasmas* **15** 012303

[32] Camenen Y. *et al* 2011 *Nucl. Fusion* **51** 073039
[33] Yoshida M. *et al* 2009 *Phys. Rev. Lett.* **103** 065003
[34] McDermott R.M. *et al* 2011 *Plasma Phys. Control. Fusion* **53** 124013
[35] Solomon W.M. *et al* 2011 *Nucl. Fusion* **51** 073010
[36] Shi Y.J. *et al* 2012 *Proc. 24th IAEA Fusion Energy Conf. (San Diego, CA, 2012)* www-pub.iaea.org/MTCD/Meetings/PDFplus/2012/cn197/cn197_Programme.pdf
[37] Sun A.P. 2012 *Proc. 2nd Asia Pacific Transport Working Group* (*Chengdu, China, 2012*) www.swip.ac.cn/2012aptwg/program.htm
[38] Angioni C. *et al* 2011 *Phys. Rev. Lett.* **107** 215003
[39] LaBombard B. *et al* 2004 *Nucl. Fusion* **44** 1047
[40] Rice J.E. *et al* 2005 *Nucl. Fusion* **45** 251
[41] Fedorczak N. *et al* 2012 *Nucl. Fusion* **52** 103013
[42] Ozawa H. *et al* 2003 *Rev. Geophys.* **41** 1018
[43] Rüdiger G. 1989 *Differential Rotation and Stellar Convection Sun and Solar-Type Stars* (Berlin: Akademie-Verlag)
[44] Ida K. *et al* 1998 *J. Phys. Soc. Japan.* **67** 4089
[45] Ku S. *et al* 2012 *Nucl. Fusion* **52** 063013
[46] Wang W.X. *et al* 2011 *Phys. Plasmas* **18** 042502
[47] Gürcan Ö.D. *et al* 2012 *Joint EU-US TTF Meeting* (*Padova, Italy 2012*) www.igi.cnr.it/eu_us_ttf_2012/sites/default/files/attachments/BookOfAbstracts.pdf
[48] Moffatt K.H. 1978 *Magnetic Field Generation in Electrically Conducting Fluids* (Cambridge: Cambridge University Press) p 353
[49] Frisch U. *et al* 1987 *Physica* D **28** 382
[50] McDevitt C.J. *et al* 2009 *Phys. Rev. Lett.* **103** 205003
[51] Diamond P.H. *et al* 2005 *Plasma Phys. Control. Fusion* **47** R35
[52] Dominguez R.R. *et al* 1993 *Phys. Fluids* B **5** 3876
[53] Gürcan Ö.D. *et al* 2007 *Phys. Plasmas* **14** 042306
[54] Gürcan Ö.D. *et al* 2010 *Phys. Plasmas* **17** 112309
[55] Kwon J.M. *et al* 2012 *Nucl. Fusion* **52** 013004
[56] Diamond P.H. and Kim Y.-B. 1991 *Phys. Fluids* B **3** 1626
[57] Taylor G.I. 1915 *Phil. Trans. R. Soc. Lond.* A **215** 1
[58] Diamond P.H. *et al* 2008 *Plasma Phys. Control. Fusion* **50** 124018
[59] Scott B. and Smirnov J. 2010 *Phys. Plasmas* **17** 112302
[60] Brizard A.J. and Tronko N. 2011 *Phys. Plasmas* **18** 082307
[61] Abiteboul J. *et al* 2011 *Phys. Plasmas* **18** 082503
[62] Galeev A.A. and Sagdeev R.Z. 1979 *Reviews of Plasma Physics* vol 6, ed M.A. Leontovich (New York: Consultants Bureau)
[63] Diamond P.H., Itoh S.-I. and Itoh K. 2010 *Modern Plasma Physics* vol 1 (*Physical Kinetics of Turbulent Plasmas*) (Cambridge: Cambridge University Press)
[64] Dimitri Mihalas and Barbara Weibel-Mihalas 1999 *Foundations of Radiation Hydrodynamics* (New York: Courier Dover Publications)
[65] Bühler O. 2009 *Waves and Mean Flows* (Cambridge: Cambridge University Press)
[66] Carlstrom T.N. *et al* 2002 *Plasma Phys. Control. Fusion* **44** A333
[67] Hennequin P. *et al* 2010 *European Physical Society* vol 34A P1.1040 http://ocs.ciemat.es/EPS2010PAP/pdf/P1.1040.pdf
[68] Catto P.J. *et al* 1973 *Phys. Fluids* **16** 1719 http://pof.aip.org/resource/1/pfldas/v16/i10/ p1719_s1
[69] Ida K. *et al* 2012 *Proc. 24th IAEA Fusion Energy Conf.* (*San Diego, CA, 2012*) www-pub.iaea.org/MTCD/Meetings/PDFplus/2012/cn197/cn197_Programme.pdf
[70] Dif-Pradalier G. *et al* 2010 *Phys. Rev.* E **82** 025401(R)
[71] Politzer P.A. 2000 *Phys. Rev. Lett.* **84** 1192
[72] Messiaen A. *et al* 1996 *Phys. Rev. Lett.* **77** 2487
[73] Messiaen A. *et al* 1997 *Phys. Plasmas* **4** 1690
[74] Wang W.X. *et al* 2010 *Phys. Plasmas* **17** 072511
[75] Gürcan Ö.D. *et al* 2010 *Phys. Plasmas* **17** 032509
[76] Snyder P.B. *et al* 2009 *Nucl. Fusion* **49** 085035
[77] Jhang H. *et al* 2012 *Proc. 24th IAEA Fusion Energy Conf.* (*San Diego, CA, 2012*) www-pub.iaea.org/MTCD/Meetings/PDFplus/2012/cn197/cn197_Programme.pdf p 281
[78] deGrassie J.S. 2009 *Plasma Phys. Control. Fusion* **51** 124047
[79] Kim S.S. *et al* 2011 *Nucl. Fusion* **51** 073021
[80] Coppi B. *et al* 1967 *Phys. Fluids* **10** 582
[81] Horton W. *et al* 1981 *Phys. Fluids* **24** 1077
[82] Garbet X. *et al* 2001 *Phys. Plasmas* **8** 2793
[83] Garbet X. *et al* 2002 *Phys. Plasmas* **9** 3893
[84] Rettig C.L. *et al* 2001 *Phys. Plasmas* **8** 2232
[85] Naulin V. 2012 *Joint EU-US TTF Meeting* (*Padova, Italy, 2012*) www.igi.cnr.it/eu_us_ttf_2012/sites/default/files/attachments/BookOfAbstracts.pdf
[86] Kwon J.M. *et al* 2011 *Plasma Conf. 2011* (*Kanazawa, Japan, 2011*) www.jspf.or.jp/PLASMA2011/eng/contents04a.html
[87] deGrassie J.S. 2004 *Phys. Plasmas* **11** 4323
[88] Wang L. and Diamond P.H. 2013 *Phys. Rev. Lett.* **110** 265006
[89] Rice J.E. *et al* 2013 *Phys. Rev. Lett.* **111** 125003